

RESEARCH

IGF2 drives formation of ileal neuroendocrine tumors in patients and mice

Tanupriya Contractor¹, Richard Clausen¹, Grant R Harris¹, Jeffrey A Rosenfeld², Darren R Carpizo², Laura Tang³ and Chris R Harris^{1,2,4}

¹Raymond and Beverly Sackler Foundation, New Brunswick, New Jersey, USA

²Rutgers Cancer Institute of New Jersey, New Brunswick, New Jersey, USA

³Department of Pathology, Memorial Sloan Kettering Cancer Center, New York, New York, USA

⁴Department of Surgery, Rutgers Robert Wood Johnson Medical School, New Brunswick, New Jersey, USA

Correspondence should be addressed to C R Harris: harrisch@cinj.rutgers.edu

Abstract

By the strictest of definitions, a genetic driver of tumorigenesis should fulfill two criteria: it should be altered in a high percentage of patient tumors, and it should also be able to cause the same type of tumor to form in mice. No gene that fits either of these criteria has ever been found for ileal neuroendocrine tumors (I-NETs), which in humans are known for an unusual lack of recurrently mutated genes, and which have never been detected in mice. In the following report, we show that I-NETs can be generated by transgenic RT2 mice, which is a classic model for a genetically unrelated disease, pancreatic neuroendocrine tumors (PNETs). The ability of RT2 mice to generate I-NETs depended upon genetic background. I-NETs appeared in a B6AF1 genetic background, but not in a B6 background nor even in an AB6F1 background. AB6F1 and B6AF1 have identical nuclear DNA but can potentially express different allelic forms of imprinted genes. This led us to test human I-NETs for loss of imprinting, and we discovered that the *IGF2* gene showed loss of imprinting and increased expression in the I-NETs of 57% of patients. By increasing IGF2 activity genetically, I-NETs could be produced by RT2 mice in a B6 genetic background, which otherwise never developed I-NETs. The facts that *IGF2* is altered in a high percentage of patients with I-NETs and that I-NETs can form in mice that have elevated IGF2 activity, define *IGF2* as the first genetic driver of ileal neuroendocrine tumorigenesis.

Key Words

- ▶ carcinoids
- ▶ neuroendocrine tumours

Endocrine-Related Cancer
(2020) **27**, 175–186

Introduction

Neuroendocrine tumors (NETs) can occur throughout the body, within the many organs that contain hormone-producing cells. Tumors found in these various locations can share common genetic drivers, as indicated by the fact that patients inheriting certain alleles of the *MEN1* or *MEN2/RET* genes can develop neuroendocrine tumors in multiple locations, including pancreas, pituitary, thyroid, parathyroid, duodenum, thymus, adrenals and/or

lungs (Wells *et al.* 2013, Kamilaris & Stratakis 2019). But familial syndromes account for only about 10% of the clinical cases of NETs (Scarpa 2019), while the other 90% of patients develop sporadic NETs that occur in single organs. Deep sequencing has identified genes that are recurrently mutated in many of the organ-specific, sporadic NETs. For instance, in sporadic pancreatic NETs (PNETs), recurrent mutations are observed in *MEN1*,

DAXX or *ATRX* (Jiao *et al.* 2011). *MEN1* loss also promotes PNET formation in mice (Crabtree *et al.* 2001). The fact that *MEN1* is lost in a high percentage of patient samples and that *MEN1* loss also causes PNETs to develop in mice defines this gene as a genetic driver of PNETs, and *MEN1* is likely a driver of many other types of NETs as well.

But *MEN1* is not a genetic driver of all types of NETs, including ileal NETs (I-NETs). I-NETs are the most common tumors of the small intestine. Approximately 2500 new cases of I-NETs occur in the United States every year (Dasari *et al.* 2017), and not only is the overall incidence of I-NETs increasing, but more importantly the percentage of patients with metastatic I-NETs at initial diagnosis is also increasing (Halperin *et al.* 2017). Metastatic I-NETs can be very aggressive, replacing as much as 80% of a patients' normal liver. The genetic driver of this disease has long remained a mystery. Ileal neuroendocrine tumors are not found in patients with any of the multiple endocrine tumor syndromes, do not have mutations in the *MEN1* and *MEN2/RET* genes that determine familial endocrine tumor syndromes, and do not have mutations in genes commonly mutated in other sporadic NETs such as *ATRX* or *DAXX*. Nor do I-NETs have mutations in oncogenes or tumor suppressor genes commonly mutated in human cancers, such as *TP53*, *RB1*, *BRCA1*, or *KRAS*. Probably the most compelling evidence for a genetic cause of I-NETs is the fact that chromosome 18 is lost in more than half of the tumors (Zhao *et al.* 2000, Wang *et al.* 2005), suggesting the presence of a key tumor suppressor gene or genes on chromosome 18. However, none of the chromosome 18 genes show recurrent mutations in I-NETs. In fact, the only gene that is recurrently mutated in I-NETs is *CDKN1B*, which is found on chromosome 12 and is mutated in 5–8% of I-NETs (Banck *et al.* 2013, Francis *et al.* 2013, Maxwell *et al.* 2015). This low percentage suggests that *CDKN1B* is not the genetic driver of I-NETs, and indeed I-NETs have not been reported in *Cdkn1b* mutant mice. The overall frequency of mutations in ileal neuroendocrine tumors is quite low (Banck *et al.* 2013, Francis *et al.* 2013) and is more similar to the low mutation frequency observed in pediatric tumors, which does not fit with the fact that I-NETs are usually detected in older patients.

Very few research tools are available to study I-NET biology. I-NETs do not easily yield patient-derived xenografts, and while I-NET cell lines have been reported (Pfragner *et al.* 1996, 2009, Kolby *et al.* 2001), these have not been made publicly available. There are also no autochthonous animal models of I-NETs. Conversely, the study of PNET biology is aided by the existence of several autochthonous mouse models (Hanahan 1985, Crabtree *et al.* 2001, Du *et al.* 2007,

Shen *et al.* 2009, Contractor *et al.* 2016, Wong *et al.* 2020), by publicly-available cell lines, and by knowledge of several recurrently mutated genes. For these reasons, many more research studies are published about PNETs than I-NETs, in spite of the fact that the clinical frequencies of the two diseases are roughly the same (Dasari *et al.* 2017). Knowledge about a genetic driver of I-NETs, and availability of a mouse model for this disease, could stimulate research interest in ileal neuroendocrine tumors.

Among the many mouse models of pancreatic NETs is the transgenic model RT2 (Hanahan 1985), which has proven to be unusually versatile for the modeling of neuroendocrine tumors. Originally developed as a model of insulinomas, RT2 mice can also model a different NET subtype, nonfunctioning pancreatic neuroendocrine tumors, if the genetic background is changed from B6 to AB6F1 (Kobayashi *et al.* 2019). In a third genetic background, B6D2F1, RT2 mice can also generate a third type of NET, duodenal NETs (Grant *et al.* 1991). In this report, we demonstrate that in yet another genetic background, RT2 mice can develop ileal neuroendocrine tumors. Analysis of this first I-NET animal model also allowed identification of the first I-NET driver gene.

Materials and methods

Mouse experiments

Mouse experiments were approved by the Institutional Animal Care and Use Committee of Rutgers University. Mouse husbandry protocols have been previously described (Contractor *et al.* 2016). RT2 B6 mice were obtained from the National Cancer Institute (Frederick, MD), and A/J and B6 *Igf1bp1*(+/-) mice were purchased from Jackson Laboratories. RT2 AB6(F1) animals were generated by mating RT2B6 males to A/J females, and RT2 B6A(F1) animals were generated by mating RT2B6 females to A/J males. Female B6 *Igf1bp1*(-/-) mice were mated to male RT2B6 to generate RT2B6 *Igf1bp1*(+/-) animals. Animals were killed using CO₂ asphyxiation and cervical dislocation at 17 weeks of age. Pancreatic tumor volume was measured using a caliper, and livers were examined for metastasis. Intestinal tracts were analyzed for lesions within the lumen of the organs. Tumors were flash frozen and/or preserved in formalin.

Whole exome sequencing

Mouse DNA was prepared from tail, PNET or I-NET tissue using a Promega Wizard Kit. SureSelectXT Mouse All Exon

Kit (Agilent) was used for capture of exonic DNA from the mouse samples. DNA was sequenced on an Illumina machine for 150 bp paired-end sequencing according to standard protocols. Reads were aligned to the mouse reference genome (mm9) with BWA 0.78-r455 (Li & Durbin 2009). Germline SNPs were called using GATK v3.8 (DePristo *et al.* 2011) and somatic SNPs were called using Mutect 11.4 (Cibulskis *et al.* 2013). Samples were manually compared for common mutations.

F2 analysis

A SNP assay for rs31828088 was designed and synthesized by ThermoFisher. The sequences of the outside primers were 5'AGCCCACCACAGCTGAAC and 5'CACAAGTCCAGGATATGTCTGAGAA. Reporter 1 sequence was 5'VIC-ACACTCGATAACATCTTGT-NFQ and reporter 2 sequence was 5'FAM-CACTCTGATAACGTC TTGT-NFQ. This assay was used to genotype DNAs from 279 RT2 AB6(F2) mice, which were previously reported (Contractor *et al.* 2016). Rs31828088 resides upstream of the *INS2* gene, within a cluster of imprinted genes on mouse chromosome 7qF5. The B6 lineage and the A/J lineage encode different versions of this SNP.

Sequencing analysis of *Armcx3*

By whole exome sequencing, *Armcx3* was initially judged to possess a common mutation in tumors from mouse 31462. However, this sequence was part of a 750 nt region that is duplicated on another chromosome within the mouse genome. To focus on the sequence of *Armcx3* and not on the duplicated region, DNA isolated from tail, PNET and INET of mouse 31462 was subjected to PCR to amplify a portion of the genome that was specific to the *Armcx3* gene and not part of the duplicated region. PCR primers were 5'-CCAGGAGCTTGTGATGAACG-3' and 5'-AGCCCTTTTCTGTACAGCTCT-3'. After 40 cycles, the DNA was purified using a column from Qiagen. Sanger sequencing was primed using the oligonucleotide 5'-GACTGCAGGTCTGGTGATTG-3' and was performed by Genewiz Inc.

Copy number analysis of *Cdhr2*

By whole exome sequencing, *Cdhr2* was initially judged to have a copy number of 3 in tumors from mouse 31462. To analyze this further, DNA isolated from tail, PNET and INET of mouse 31462 was subjected to copy number analysis using real-time RTPCR. Assay Mm00392193_cn

(ThermoFisher) binds within the putative amplified region and was used to analyze the copy number of *Cdhr2*. DNA copy number was normalized using an assay against *Tfrc* (ThermoFisher).

Analysis of RNA

Flash-frozen mouse tumors were minced in TRIzol (ThermoFisher) and homogenized using a Polytron 1200E. Chloroform was then added and the upper aqueous phase was removed after microcentrifugation. Ethanol was added, and RNA was isolated using an RNeasy column (Qiagen). RNA was converted into cDNA using RT reagents (ThermoFisher). qPCR was performed, using a Prism 7500 (Applied Biosystems). TaqMan assays for *Igf2* and beta-actin were purchased from ThermoFisher. The following assays were designed with Primer3 software (<http://bioinfo.ut.ee/primer3/>) and used with SYBR green reagents (ThermoFisher): *H19* 5'ATCTGCTCCAAGGTGAAGCT and 5'GAAGTCATCCCGGGGTAGAG; *H19os* (A) 5'CTATATGGGGATGGTGTCCAG and 5'GCCTAGTCT GAGCCCTGTTG; *H19os* (B) 5'TTTGCCAGCACACAA TGTC A and 5'CACCCCATCTTTCAGACCCT; *Ascl2* 5'GGAGCTGCTTGACTTTTCCA and 5'TTTGGTCAGGCT GCACTAGA; *Tnfrsf26* 5'CGTACAGCTGATCGTGTGTG and 5'CTGTCTGGCTCTGAGTCAA; *Tnfrsf23* 5'TCAACTGTCCCGATGGTGAA and 5'GTTCAATCAT GCAGGCCA; *Tnfrsf22* 5'CTCCTTCAAATGTCCCCTG and 5'TGTTCTGGGTGACACTTCT; *Th* 5'AAACCCTCC TCACTGTCTCG and 5'CGCACAAAGTACTCCAGGTG; *Cd81* 5'CAGTTCTATGACCAGGCCCT and 5'TGAGTATGT TGCCGCCTGA; *Tssc4* 5'CCAAGTGTGTCCCCAGAGA and 5'GGTAGAACTCATGCCTCGGA; *Kcna1* 5'CCTCAT CGTGGTTGTAGCCT and 5'AAGCGGATACCC CTGATAGC; *Scl22A18* 5'CCATCCTGGCTTTTGTGGTC and 5'ATACACTGGCCTTGTTCCA; *Phlda2* 5'CGCTCT GGGTCCGTGAAA and 5'GGGGCAAGGCTCAGCAAG; *Cdkn1c* 5'GCCAATGCGAACGACTTCTT and 5'ACG TTTGGAGAGGGACACC; and *Napil4* 5'GTCTTTCAG ATGGAGGCCCT and 5'AAGACGTTCTGCAAAGCTG.

Immunohistochemistry

Antibodies were purchased from the following suppliers: secretin (LSBio); chromogranin A (Abcam); serotonin (Immunostar); insulin (Agilent); and CDX2 (Cell Signaling). For antigen retrieval, slides were boiled for 16 min in 0.93% (v/v) Antigen Unmasking Solution H3301 (Vector Labs), then slowly cooled to room temperature for 30 min. Secondary antibodies were purchased from

Vector Labs and diluted 500-fold in 10% goat serum and 1% BSA. Slides were treated with Vectastain Elite ABC peroxidase kit (Vector Labs) for 30 min, then treated with ImmPact DAB peroxidase substrate (Vector Labs SK-4105). The slides were counterstained with hematoxylin (Vector Labs). Immunohistochemistry results were evaluated by a pathologist (LT) with expertise in neuroendocrine tumors.

Statistical analysis

GraphPad Prism 7.04 software was used for analysis. Two-tailed *t*-test was used to evaluate RNA expression from sets of mouse and human tumors. Fisher's exact test was used to compare metastasis frequencies. Nonparametric Mann-Whitney analysis was used to evaluate tumor volumes. Outliers were identified by Rout analysis ($q=1\%$).

Analyses of human tumor samples

Human ileal neuroendocrine tumors and matched normal tissues were provided by the Cooperative Human Tissue Network (CHTN), which obtained informed consents from patients. Analyses of human tumor samples were approved by the Institutional Review Board of CHTN.

Analysis of imprinting

Genomic DNA was prepared from frozen human tumors or matched normal tissue using a Wizard DNA prep kit (Promega). RNA was prepared from tumor or normal tissue using an RNAeasy kit following TRIzol extraction. RNA was converted into cDNA using reverse transcriptase reagents from ThermoFisher, or else as a negative control reverse transcriptase was omitted from the reaction. Primers 5'CTC TGT CCT CCC CTC CTT TG 3' and 5' AAC ACC CCA CAA AAG CTC AG 3' were used to amplify the sequence flanking the rs680 SNP within the *IGF2* coding sequence. Primers 5'CGG ACA CAA AAC CCT CTA GC 3' and 5'GTC GTG GAG GCT TTG AAT CTC 3' were used to amplify the sequence around the rs10840159 SNP within the *H19* sequence. Amplifications from cDNA were performed for no more than 40 cycles in order to avoid genomic contamination. Following amplification, PCR products were enzymatically digested using ApaI (rs680 SNP) or MscI (rs10840159 SNP), then analyzed by agarose gel electrophoresis.

Pyrosequencing

Genomic DNA was treated with bisulfite, then subjected to pyrosequencing assays targeted against DMR0, DMR2 and

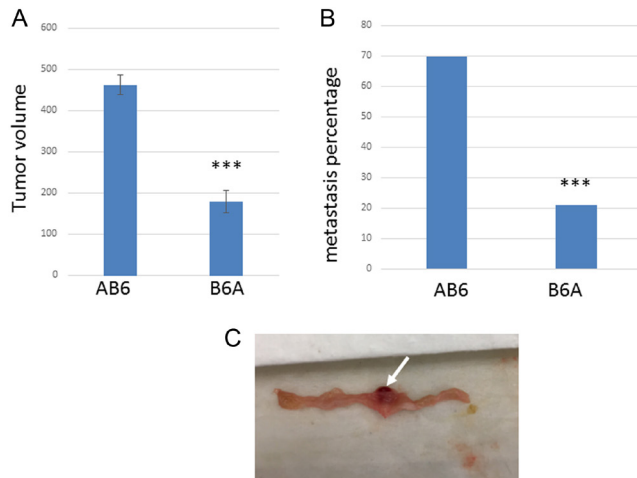
H19 IGR. Pyrosequencing was performed by EpigenDx Inc (Hopkinton, MA, USA), using EpigenDx assays ADS1051, ADS006, and ADS596.

Results

Mouse modeling of I-NETs

In a previous study, RT2 AB6(F1) animals were generated by mating RT2 B6 males with A/J females; these animals produced highly metastatic, non-functioning pancreatic NETs (NF-PNETs) (Kobayashi *et al.* 2019). The reverse cross, in which A/J males were mated to RT2 B6 females, generates a slightly different line denoted RT2 B6A(F1); this mating was technically more challenging because RT2B6 mothers were extremely hypoglycemic and often died before or shortly after birth. But several litters of RT2 B6A(F1) mice were generated by fostering the pups to other mothers, and once these animals reached adulthood it became obvious that RT2 B6A(F1) mice had three phenotypes that were distinct from the nearly genetically identical RT2 AB6(F1) animals. First, pancreatic NETs produced by RT2 B6A(F1) were much smaller (Fig. 1A); second, liver metastasis was less common in RT2 B6A(F1) (Fig. 1B); and third, small, highly vascular tumors appeared within the ileum of the small intestines of RT2 B6A(F1) mice but not in RT2 AB6 (F1) mice (Fig. 1C). Thirty age-matched male RT2 B6AF(F1) animals were evaluated and 12 were found to have ileal tumors. Single ileal tumors were detected in nine of the animals, while each of the other animals had two ileal tumors. Pathological and immunohistochemical analysis revealed the ileal tumors to be neuroendocrine (Fig. 2A and B). Serotonin, a marker of human I-NETs, was detected in 22% of mouse ileal neuroendocrine tumors (Fig. 2C). The ileal tumors did not express secretin or insulin, which are common markers of duodenal and pancreatic NETs, respectively (Fig. 2D and E).

We suspected that the ileal tumors in RT2 B6A(F1) mice might be primary ileal neuroendocrine tumors, which is a disease that has never previously been observed in mice. But it was also possible that the ileal tumors were metastatic lesions that originated from the primary PNETs generated by these animals; however, this seemed less likely because ileal tumors were not observed in the more metastatic RT2 AB6(F1) model (Fig. 1B). To test whether the ileal tumors were primary tumors, we employed two methods. First, immunohistochemistry was used to test for expression of the small intestinal marker CDX2; this test is often used on patient samples to distinguish whether a

**Figure 1**

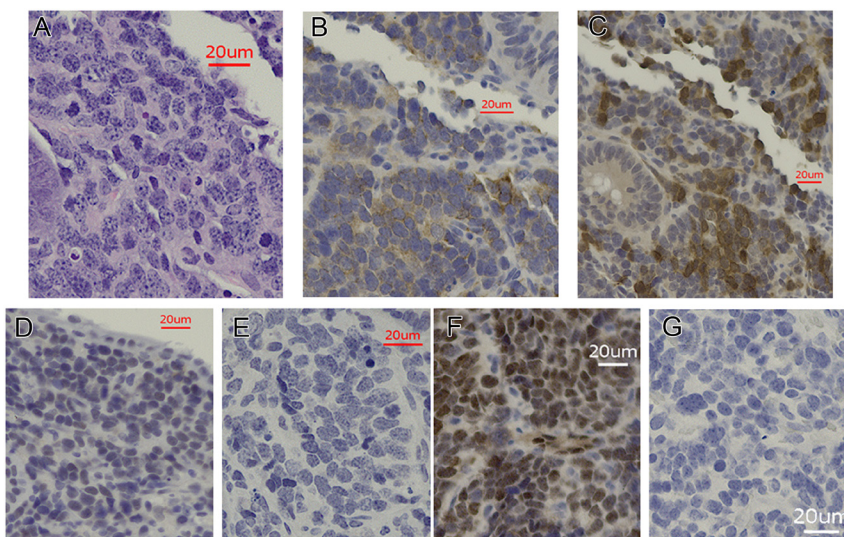
Phenotypic differences between RT2 AB6(F1) and RT2 B6A(F1) mice. (A) Comparison of pancreatic neuroendocrine tumor volume in age-matched RT2 mice from different genetic backgrounds (AB6F1 or B6AF1). 334 RT2 AB6(F1) and 46 RT2 B6A(F1) were evaluated. *** indicates a *P* value below 0.001 by Mann-Whitney analysis. (B) Comparison of liver metastasis frequency in age-matched RT2 mice with AB6F1 or B6AF1 genetic backgrounds. *** indicates a *P* value below 0.001 by Fisher's exact test. (C) A section of mouse ileum, with tumor indicated by arrow. A full colour version of this figure is available at <https://doi.org/10.1530/ERC-19-0505>.

liver metastasis from an unknown primary NET originated from a primary PNET or lung NET, which do not express CDX2, or from a primary I-NET, which does express CDX2 (Strosberg *et al.* 2017). As shown in Fig. 2F and G, the mouse ileal tumors expressed the ileal NET-specific marker CDX2, while the mouse PNETs did not. Second, whole exome sequencing was performed on PNETs and ileal tumors isolated from the same two animals, because metastatic tumors should have mutations in common with precursor primary tumors, whereas independently arising

primary tumors should not share common mutations. In tumors isolated from mouse 31508, there were no common mutations, indicating that the ileal tumor in this animal is a primary I-NET (Supplementary Fig. 1, see section on [supplementary materials](#) given at the end of this article and see also Supplementary Table 1 for nonsynonymous mutations and Supplementary Table 2 for copy number variations. Synonymous mutations are not shown). For a second mouse, identified as number 31462, initial analysis of whole exome sequencing data suggested the presence of two common mutations, a nonsynonymous SNP and a copy number variation (Supplementary Tables 3 and 4). However, further analysis revealed that both of the common mutations were actually false positives: the copy number amplification could not be found by real-time RTPCR analysis of the same region, and a C177A mutation could not be detected in the *Armcx3* genes of either tumors using Sanger sequencing (Supplementary Figs 2 and 3). The *Armcx3* sequence is part of a very long repeat that is also found in another part of the mouse genome, which was likely responsible for the false-positive result. Thus, the ileal tumor from mouse 31462 also arose independently from the PNET and is likely a primary ileal neuroendocrine tumor.

Loss of imprinting of *IGF2* in human I-NETs

At the nuclear DNA level, the RT2 B6A(F1) line that develops I-NETs is identical to the RT AB6(F1) line that does not develop I-NETs. But since the lineage of the parents is reversed in these lines, I-NET formation might be caused by one or more imprinted genes, which are genes in which only the allele contributed by the father

**Figure 2**

Pathological analysis of ileal tumors from RT2B6AF1 mice. (A) Hematoxylin and eosin staining of an ileal tumor from an RT2 B6A(F1) animal. (B, C, D and E) Immunohistochemical analysis of Chromogranin A (B), serotonin (C), secretin (D) and insulin (E) by an ileal tumor from an RT2 B6A(F1) mouse. (F and G) Immunohistochemical comparison of CDX2 expression by an I-NET (F) and a PNET (G) isolated from the same RT2 B6A(F1) mouse.

or by the mother is expressed. We also hypothesized that if an imprinted gene is required for I-NET formation in mice, then an imprinted gene might also be required for I-NET formation in patients. So we decided to analyze human I-NETs for loss of imprinting (LOI) of *IGF2*, as *IGF2* LOI has been associated with several types of tumors (Leick *et al.* 2012) but has not previously been assessed for I-NETs.

We identified 30 I-NET patients that were heterozygous for SNP rs680, which occurs within the transcribed portion of the *IGF2* gene. Heterozygotes encoded one allele with a recognition site for the *ApaI* restriction endonuclease, and a second allele that lacks this recognition site. cDNA from the tumors of heterozygotes was amplified by PCR, and the PCR products were treated with *ApaI*. Agarose gel electrophoresis revealed that 17 out of 30 tumors expressed both alleles of *IGF2*, indicating loss of imprinting (Fig. 3A). *IGF2* sequences could only be detected in samples treated with reverse transcriptase (Supplementary Fig. 4), eliminating the possibility of genomic DNA contamination.

As would be expected, loss of imprinting correlated with increased *IGF2* transcription (Fig. 3B). LOI of *IGF2* has previously been linked to DNA methylation of three regions, which are called DMR0, DMR2 and H19 IGR (Dejeux *et al.* 2009). DMR0 and DMR2 are within the *IGF2* gene, and H19 IGR is near the adjacent gene, *H19*. Pyrosequencing analysis of bisulfite-treated tumor DNA showed no difference in DNA methylation of H19 IGR, but both DMR0 and DMR2 were more methylated in tumors from patients showing LOI (Fig. 3C). Increased methylation of DMR2 has also been linked to loss of *IGF2* imprinting for another type of neuroendocrine tumor, insulinomas (Dejeux *et al.* 2009).

The *H19* gene near *IGF2* is also an imprinted gene. We identified 15 I-NET patients that were heterozygous for SNP rs1081459, which is found within the transcribed region of *H19*. One allele of this SNP produces a recognition site for the *MscI* enzyme, and the second allele does not. *MscI* digestion of PCR products from tumor cDNAs revealed no loss of imprinting of *H19* in any of the ileal tumor samples (Supplementary Fig. 5). Therefore, loss of imprinting in patients with ileal neuroendocrine tumors was specific for the *IGF2* gene, and did not reflect a general loss of control of genetic imprinting in I-NETs.

Matched normal tissue was available for 12 of the patients that showed *IGF2* LOI. In all 12 cases, loss of imprinting of *IGF2* was present not just in the tumor but also in the normal tissue (Fig. 3D). There was also increased transcription of *IGF2* in the matched normal

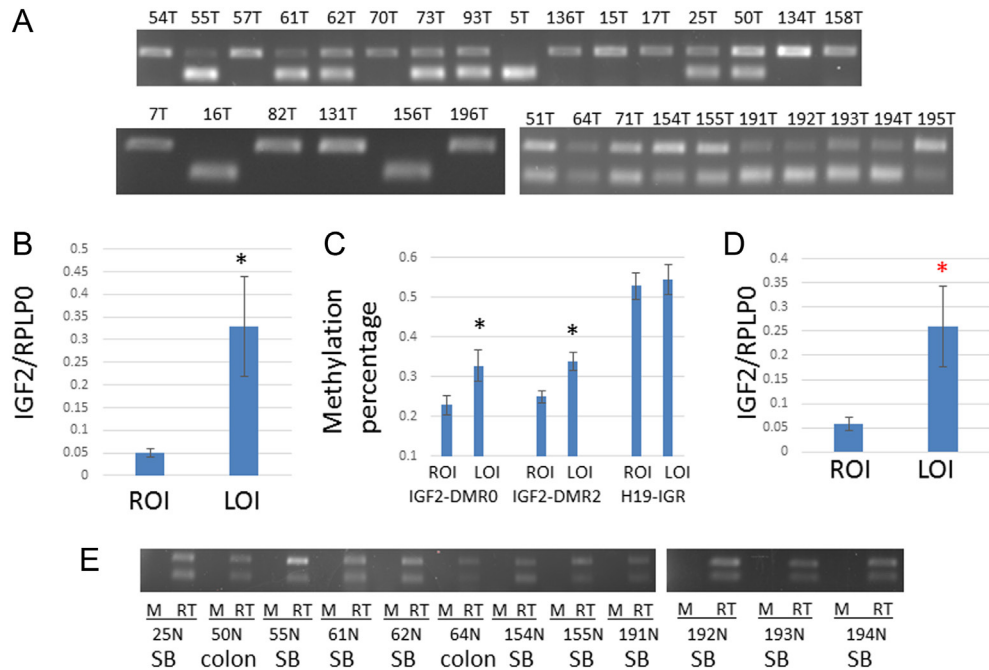
tissue from patients showing loss of imprinting (Fig. 3E). For 10 of the 12 cases in which *IGF2* LOI was observed in matched normal tissue, both tumor and normal tissue originated from the small intestine, but the distance between tumor and the matched normal tissue was not recorded. However in the other two cases, the tumor was removed from the small intestine while the normal was removed from the large intestine. The pathology report for patient 50N was particularly detailed. The ileal tumor of this patient was removed 20 cm from the junction between the small and large intestine, while the matched normal was removed from an undescribed area within the large intestine. Thus for this patient, *IGF2* LOI likely occurred across a 20 cm or larger region of the intestinal tract.

Effect of *Igfbp1* on I-NET formation in mice

The high percentage of patients with LOI of *IGF2* suggests that *IGF2* is a genetic driver of ileal neuroendocrine tumorigenesis. But by the strictest of definitions, a genetic driver should not only be altered in a majority of patient tumors, but should also be able to drive formation of the same tumors in mice. To test whether *Igf2* can promote I-NETs *in vivo*, we examined the effects of increased IGF2 activity in RT2 B6 mice. This mouse line ordinarily does not generate I-NETs. To increase IGF2 activity, male RT2 B6 mice were mated to female B6 *Igfbp1*($-/-$) animals to create a generation of RT2 B6 *Igfbp1*($+/-$) mice. *Igfbp1* encodes a protein that prevents IGF2 from binding to its receptor (Kajimura *et al.* 2005, Baxter 2014); therefore, a decrease in copy number of *Igfbp1* should lower expression of IGFBP1 and thereby increase the effective activity of IGF2 in RT2B6 *Igfbp1*($+/-$) mice relative to RT2B6 animals. As shown in Supplementary Fig. 6, RT2B6 *Igfbp1*($+/-$) mice indeed had decreased expression of *Igfbp1*, as measured in PNETs isolated from both lines.

A high proportion (38.5%) of RT2B6 *Igfbp1*($+/-$) mice developed ileal tumors, which expressed chromogranin A and CDX2 (Supplementary Fig. 7). This result strongly supports *Igf2* as a genetic driver of ileal neuroendocrine tumorigenesis.

The RT2 B6 and RT2B6 *Igfbp1*($+/-$) mice were also assessed for pancreatic neuroendocrine tumor volume and for liver metastasis, as these were two other phenotypic differences that appeared to be affected by an imprinted gene in RT2 B6A(F1) mice (Fig. 1A and B). Indeed, the RT2 B6 *Igfbp1*($+/-$) animals not only developed I-NETs but also showed clear decreases in PNET volume and in

**Figure 3**

Analysis of IGF2 imprinting in human ileal neuroendocrine tumor samples. (A) Tumor cDNA from patients heterozygous for the rs680 SNP in IGF2 were PCRd with primers that flanked the SNP. The DNA was then treated with restriction endonuclease Apal, which digests in the middle of the PCR product produced by one of the alleles but which can not digest the other allele. Patient samples that show only one band, large or small, have retained imprinting, whereas patient samples that show both bands have lost imprinting. 5T and 136T are homozygous controls. (B) *IGF2* transcription was compared in tumor samples from patients with loss of imprinting (LOI) or with retention of imprinting (ROI). Expression of *IGF2* mRNA was quantified by Q-PCR. Statistical significance was determined by two-tailed *T* test. A total of 22 samples (11 with loss of imprinting and 11 with retention of imprinting) were analyzed. *RPLPO* was used as a normalization control. * indicates a *P* value below 0.05 by two tailed *t*-test. (C) DNA methylation within three regions that have previously been linked to *IGF2* imprinting were analyzed by pyrosequencing. Eighteen tumor DNAs were compared, ten from patients without loss of imprinting and eight from patients showing loss of imprinting. Methylation percentages within each assay were analyzed using two-tailed *T* test, and * indicates a *P* value below 0.05. (D) Expression of *IGF2* mRNA by normal adjacent tissue was quantified by Q-PCR. The samples were classified according to whether or not the patients showed loss of imprinting. A total of 18 samples, 10 of which had LOI, were analyzed. *RPLPO* was used as a normalization control. Statistical significance was determined by two-tailed *T* test. * indicates a *P* value below 0.05. (E) cDNA was prepared from normal tissue available from patients showing loss of imprinting of *IGF2* in tumor tissue. Imprinting was determined by PCR amplification around SNP rs680, followed by digestion with the restriction endonuclease Apal. Presence of two bands indicates loss of imprinting. The location of the normal tissue is indicated. SB indicates small bowel tissue. RT indicates that the sample was treated with reverse transcriptase, and M indicates that the sample was mock treated with no enzyme. A full colour version of this figure is available at <https://doi.org/10.1530/ERC-19-0505>.

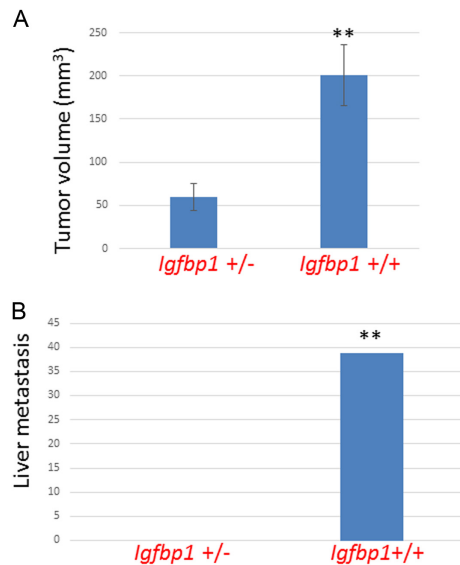
liver metastasis compared to RT2 B6 mice (Fig. 4A and B). These data suggest that an increase in IGF2 activity can drive I-NET formation while also decreasing growth and metastasis of PNETs.

Genetic association of IGF2/H19os to PNET phenotypes

Finally we also examined whether *Igf2* or a related gene associated genetically with the PNET volume and liver metastasis phenotypes observed in RT2 mice that were F1 hybrids of the inbred B6 and A/J lines (Fig. 1A and B). In mice, *Igf2* is part of a cluster of imprinted genes on chromosome 7qF5. A small nucleotide difference that distinguished chromosome 7qF5 of the A/J and B6 lineages was genotyped in DNAs from a previously

described dataset of 279 RT2 AB6(F2) hybrid animals (Contractor *et al.* 2016). RT2 AB6(F2) mice had to be used instead of F1 mice for this linkage analysis because all of the mice in the F1 generation have identical genotypes, whereas animals in the F2 generation have genetic variability that may possibly associate with phenotypes. For this study only liver metastasis and PNET volume could be compared because I-NET incidence had not been examined in this older data set.

As shown in Fig. 5A and B, the genotype of 7qF5 linked to liver metastasis and PNET volume, respectively. Animals that inherited two copies of this chromosomal segment from the A/J genetic background were more likely to have larger PNETs and liver metastasis. Heterozygotes were not considered for this analysis because in this dataset there was no way to tell which imprinted

**Figure 4**

Effect of loss of copy of *Igfbp1* in RT2 B6 mice. (A) Comparison of pancreatic neuroendocrine tumor volume in 17-week-old mice. 38 RT2 B6 male mice and 13 RT2 B6 *Igfbp1*(+/-) male mice were evaluated. ** indicates a *P* value below 0.01 by Mann-Whitney analysis. (B) Comparison of liver metastasis in 17 week-old RT2 B6 and RT2B6 *Igfbp1*(+/-) male mice. ** indicates a *P* value below 0.01 by Fisher's exact test. A full colour version of this figure is available at <https://doi.org/10.1530/ERC-19-0505>.

allele was inherited from which parent. Figure 5C summarizes metastasis data from Figs 1B and 5A and shows that F1 and F2 animals inheriting 7qF5 from A/J or B6 mothers correlated with increased or decreased metastasis, respectively, while inheritance of 7qF5 from an A/J or B6 father had no clear association with metastasis. Figure 5C thus suggested that metastasis was influenced by a maternally imprinted gene on 7qF5. Interestingly, this would rule out *Igf2*, which is a paternally imprinted gene.

Expression of all maternally imprinted genes within chromosome 7qF5 was then compared for PNETs isolated from RT2 AB6(F1) and RT2 B6A(F1) animals. PNETs were compared instead of I-NETs because both lines make PNETs, whereas only RT2 B6A(F1) make I-NETs. Only one of the maternally imprinted genes, *H19os* (Berteaux *et al.* 2008), showed differential expression (Fig. 5D). Notably, the only known function of *H19os* is to increase expression of *Igf2* (Berteaux *et al.* 2008, Tran *et al.* 2012). *Igf2* expression was indeed elevated in the RT2 B6A(F1) PNETs that had elevated *H19os* (Fig. 5E). The most simple explanation for these data would be that RT2 B6A(F1) mice have different neuroendocrine tumor phenotypes than RT2 AB6(F1) mice due to higher expression of *Igf2*, which is caused by the presence of a more active allelic form of maternally imprinted *H19os*.

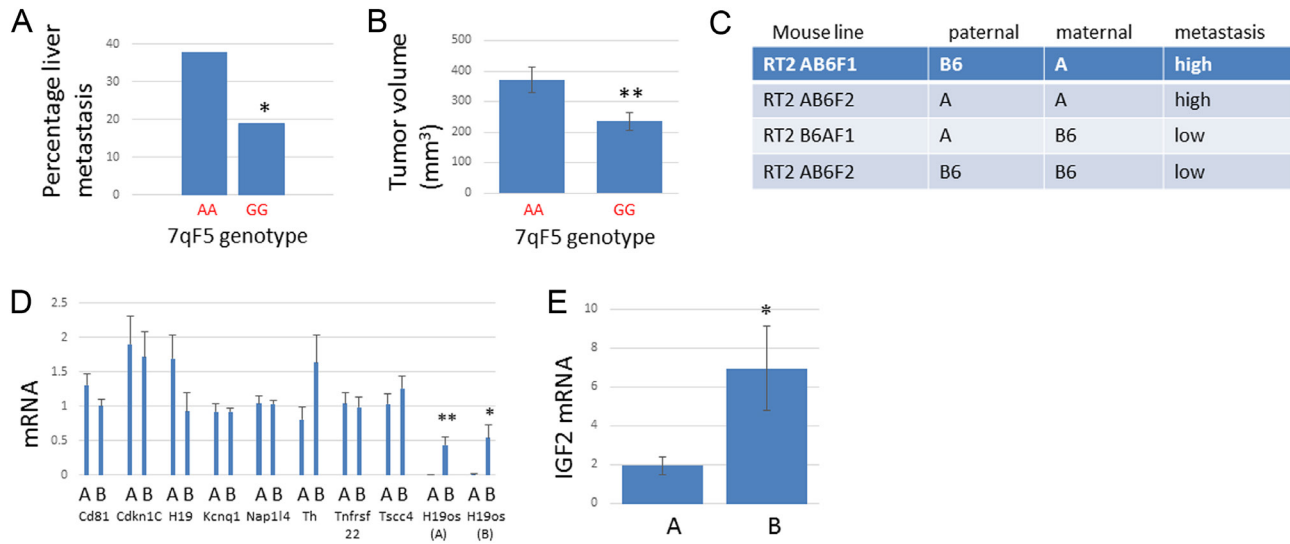
Discussion

Lack of knowledge about the genetic drivers of ileal neuroendocrine tumors has precluded attempts to model this disease by targeting specific mouse genes. Here, we were able to produce the first mouse model of I-NETs by altering the genetic background of transgenic RT2 mice to B6A(F1). Although genetic background changes have previously allowed RT2 mice to produce different types of NETs (Kobayashi *et al.* 2019), the appearance of I-NETs in RT2 B6A(F1) mice nevertheless came as a surprise; it was previously thought that these slow-growing, difficult-to-detect, genetically enigmatic tumors might be unmodelable in mice.

Interestingly, although I-NETs appeared in RT2 B6A(F1) mice, they could not be detected in nearly genetically identical RT2 AB6(F1) mice, which suggested that allelic differences in an imprinted gene could increase I-NET incidence. We investigated human I-NET samples and discovered that loss of imprinting of *IGF2* occurred in 57% of patient samples (Fig. 3A). LOI of *IGF2* is also common in other tumors of the gastrointestinal tract, for instance occurring in 47% of gastric tumors, in 32% of esophageal tumors, and in 47% of colorectal cancer (Cui 2007, Leick *et al.* 2012).

IGF2 is the first example of a gene that is altered in a majority of patients with I-NETs. Previous deep sequencing analysis of I-NETs had revealed no genes that were mutated in more than 8% of samples. Notably, loss of imprinting can be difficult to detect by deep sequencing approaches.

Patients with ileal neuroendocrine tumors generally have multiple tumors (Gangi *et al.* 2018), which can arise independently (Katona *et al.* 2006). This has suggested that mechanisms that cause multifocality, such as viral infections (Miao *et al.* 2014) or tumor-predisposing alleles (Berghthorsson *et al.* 2001), may be important drivers of I-NET tumorigenesis. Indeed, within certain families there is a predisposition to I-NETs (Sei *et al.* 2015, Du *et al.* 2016, Neklason *et al.* 2016, Dumanski *et al.* 2017), and such familial predispositions can associate with multifocality (Sei *et al.* 2015). But familial NETs tend to be rare, and the cause of non-familial multifocal I-NETs has been less clear. In this report, we found two patients in which loss of imprinting was present in both an ileal tumor and in normal large intestine, indicating that LOI can occur within a sizeable area of the intestinal tract. A large area of loss of imprinting of a secreted genetic driver protein like IGF2 may create an extended environment within which multiple I-NETs

**Figure 5**

Linkage analysis of RT2 AB6(F2) mice. For figures (A) and (B), DNAs from age-matched RT2 B6A(F2) mice were genotyped for a small nucleotide polymorphism near the *IGF2* locus. Only homozygotes were evaluated because the expressed allele of heterozygotes could not be determined. AA indicates animals that were homozygous for the allele encoded by the A/J background, which encodes adenine at the SNP position, whereas GG indicates animals that were homozygous for the allele from the B6 background, which encodes guanine. (A) Liver metastasis was compared. * indicates a *P* value below 0.05 by Fisher's exact test. (B) Tumor volumes of pancreatic NETs were compared, and ** indicates a *P* value below 0.01 by Mann-Whitney analysis. (C) This table summarizes metastatic trends of F1 animals (obtained from Fig. 1B) or F2 animals (obtained from Fig. 3A). While 7qF5 inherited from fathers did not appear to influence metastasis, F1 and F2 animals that inherited 7qF5 from A/J mothers were more likely to be metastatic than F1 and F2 animals that inherited 7qF5 from B6 mothers, respectively. (D) Comparison of RNA expression of maternally imprinted genes in the chromosome 7qF5 region of the mouse genome. Pancreatic neuroendocrine tumor extracts were used for analysis. 'A' indicates tumor extracts from RT2 AB6(F1) mice, which are less metastatic, while 'B' indicates tumor extracts from RT2 B6A(F1) mice, which are more metastatic. 18 RT2 AB6(F1) tumors and 23 RT2 B6AF(F1) tumors were evaluated. Expression was normalized to β -actin; see also Supplementary Fig. 8 for normalization to *Gapdh*. *H19os* was analyzed by two separate assays, directed against different parts of the RNA. ** indicates statistical significance ($P < 0.01$) by two-tailed *t* test and * indicates a *P* value less than 0.05. Error bars correspond to s.e.m. *Phlda2*, *Slc22A16*, *Tnfrsf23* and *Tnfrsf26* were also assayed but were poorly expressed and are not included. (E) Comparison of *Igf2* RNA expression within PNETs isolated from RT2 AB6(F1) and RT2 B6A(F1) mice. * indicates a *P* value below 0.05 by two-tailed *t*-test. Expression was normalized with β -actin. A full colour version of this figure is available at <https://doi.org/10.1530/ERC-19-0505>.

can form. Fields of loss of *IGF2* imprinting have also been reported around prostate cancers (Bhusari *et al.* 2011). In the future, it will be interesting to determine whether multifocal I-NETs are located within large areas of *IGF2* LOI.

The high incidence of loss of imprinting in human samples strongly suggested that *IGF2* is a driver of ileal neuroendocrine tumorigenesis. To test this idea further, we elevated the activity of IGF2 by removing a copy of its negative regulator, *Igf1p1*. Loss of copy of *Igf1p1* caused RT2 B6 mice, which normally do not make I-NETs, to produce I-NETs. Alteration of a gene in a high percentage of human tumors, combined with the ability of the gene to cause the same tumors to form in mice, is the strictest definition for a genetic driver.

The nearly identical lines RT2 B6A(F1) and RT2 AB6(F1) mice had other phenotypic differences in addition to differential ability to form I-NETs. Both lines developed pancreatic NETs, but these tumors were

smaller and less metastatic in the RT2 B6A(F1) line that also developed I-NETs. Interestingly, decreasing the copy number of *Igf1p1* in an RT2 B6 mouse line was sufficient to phenocopy all three of these traits: RT2 B6 *Igf1p1* (+/-) mice not only developed I-NETs, but also showed decreases in both PNET volume and liver metastasis compared to RT2 B6 mice. This suggests that IGF2, whose activity would increase due to decreased IGFBP1, not only causes I-NETs to form but can also decrease PNET metastasis. The idea that IGF2 could increase incidence of I-NETs is not surprising, given the high percentage of I-NETs with LOI of *IGF2* in Fig. 3A; however, the idea that IGF2 might decrease metastasis is less intuitive. Interestingly, expression of IGF2 is known to decrease as PNETs progress from localized disease to metastasis both in patients (Henfling *et al.* 2018) and in mice (Contractor T & Harris CR, unpublished observations). Also there are examples of other genes that have opposing effects on tumor incidence and

metastasis, including *TGF β* and *CDKN1B* (Besson *et al.* 2004, Massague 2012).

In a hybrid RT2 AB6(F2) mouse line, the phenotypes of PNET volume and liver metastasis associated with a maternally imprinted gene at mouse chromosome 7qF5 (Fig. 5). *H19os*, a maternally imprinted, positive regulator of *Igf2*, resides at this location, and expression of both *H19os* and *Igf2* was elevated in the smaller, less metastatic PNETs produced by RT2 B6A(F1) mice. Our current model is that the *H19os* allele from B6 mice is more expressed than the *H19os* allele from A/J mice, such that RT2 B6A(F1) animals that inherit this allele from their B6 mothers will have elevated expression of *Igf2*, which then leads to formation of I-NETs and to smaller, less metastatic PNETs. By this model RT2 AB6(F1) animals, which inherit the less expressed allelic form of *H19os* from their A/J mothers, would have lower expression of *Igf2*, and this would preclude formation of I-NETs but promote larger, metastatic PNETs.

Transgenic cancer mouse models, especially ones that depend upon SV40 T-antigen expression, are usually considered to be inferior to more contemporary knock-in models. The chief criticism about use of SV40 T-antigen is that this is a monkey virus protein that is not responsible for tumorigenesis in humans, while the chief criticism about use of transgenic models is that transgenes insert into incorrect genomic locations, allowing control elements from heterologous genes to drive 'leaky' expression of the transgene in heterologous cell types. But the current work demonstrates that leaky expression of SV40 T-antigen can actually be useful, particularly when little is known about the actual genetic drivers for a type of cancer. Leaky expression of T-antigen by RT2 mice has now allowed I-NETs, as well as metastatic nonfunctioning PNETs (Kobayashi *et al.* 2019), to be modeled in animals for the first time. These animal models could lead to improved clinical treatments for patients with these two highly metastatic diseases. It should be noted that there are currently no animal models for rectal carcinoids, a type of NET that arises in a disproportionate number of African-Americans (Modlin *et al.* 2003), nor for lung carcinoids, which are among the most common of all NETs (Dasari *et al.* 2017). Crossing RT2 B6 mice with additional inbred mouse lines may allow these other types of NETs to be modeled in animals.

Supplementary materials

This is linked to the online version of the paper at <https://doi.org/10.1530/ERC-19-0505>.

Declaration of interest

Chris Harris, Tanupriya Contractor and Richard Clausen were employees of the Raymond and Beverly Sackler Foundation, which is a 501c3 nonprofit. The other authors have nothing to disclose.

Funding

This work was funded by the Raymond and Beverly Sackler Foundation.

Author contribution statement

Acquisition, analysis and interpretation of data was performed by Tanupriya Contractor, Richard Clausen, Chris Harris, Laura Tang, Jeffrey Rosenfeld, and Grant Harris. Conception and design of experiments was performed by Chris Harris and Tanupriya Contractor. Writing, review and/or revision of manuscript was performed by Chris Harris, Darren Carpizo, and Tanupriya Contractor.

Acknowledgments

The authors thank Arnold Levine, Evan Vosburgh and Doug Hanahan for important discussions, Sandra Harris and Xin Yu for help with the manuscript, and the Raymond and Beverly Sackler Foundation for financial support.

References

- Bank MS, Kanwar R, Kulkarni AA, Boora GK, Metge F, Kipp BR, Zhang L, Thorland EC, Minn KT, Tentu R, *et al.* 2013 The genomic landscape of small intestine neuroendocrine tumors. *Journal of Clinical Investigation* **123** 2502–2508. (<https://doi.org/10.1172/JCI67963>)
- Baxter RC 2014 IGF binding proteins in cancer: mechanistic and clinical insights. *Nature Reviews: Cancer* **14** 329–341. (<https://doi.org/10.1038/nrc3720>)
- Bergthorsson JT, Ejlersen B, Olsen JH, Borg A, Nielsen KV, Barkardottir RB, Klausen S, Mouridsen HT, Winther K, Fenger K, *et al.* 2001 BRCA1 and BRCA2 mutation status and cancer family history of Danish women affected with multifocal or bilateral breast cancer at a young age. *Journal of Medical Genetics* **38** 361–368. (<https://doi.org/10.1136/jmg.38.6.361>)
- Berteaux N, Aptel N, Cathala G, Genton C, Coll J, Daccache A, Spruyt N, Hondermarck H, Dugimont T, Cury JJ, *et al.* 2008 A novel H19 antisense RNA overexpressed in breast cancer contributes to paternal IGF2 expression. *Molecular and Cellular Biology* **28** 6731–6745. (<https://doi.org/10.1128/MCB.02103-07>)
- Besson A, Gurian-West M, Schmidt A, Hall A & Roberts JM 2004 p27Kip1 modulates cell migration through the regulation of RhoA activation. *Genes and Development* **18** 862–876. (<https://doi.org/10.1101/gad.1185504>)
- Bhusari S, Yang B, Kueck J, Huang W & Jarrard DF 2011 Insulin-like growth factor-2 (IGF2) loss of imprinting marks a field defect within human prostates containing cancer. *Prostate* **71** 1621–1630. (<https://doi.org/10.1002/pros.21379>)
- Cibulskis K, Lawrence MS, Carter SL, Sivachenko A, Jaffe D, Sougnez C, Gabriel S, Meyerson M, Lander ES & Getz G 2013 Sensitive detection of somatic point mutations in impure and heterogeneous cancer samples. *Nature Biotechnology* **31** 213–219. (<https://doi.org/10.1038/nbt.2514>)

- Contractor T, Kobayashi S, da Silva E, Clausen R, Chan C, Vosburgh E, Tang LH, Levine AJ & Harris CR 2016 Sexual dimorphism of liver metastasis by murine pancreatic neuroendocrine tumors is affected by expression of complement C5. *Oncotarget* **7** 30585–30596. (<https://doi.org/10.18632/oncotarget.8874>)
- Crabtree JS, Scacheri PC, Ward JM, Garrett-Beal L, Emmert-Buck MR, Edgemon KA, Lorang D, Libutti SK, Chandrasekharappa SC, Marx SJ, *et al.* 2001 A mouse model of multiple endocrine neoplasia, type 1, develops multiple endocrine tumors. *PNAS* **98** 1118–1123. (<https://doi.org/10.1073/pnas.98.3.1118>)
- Cui H 2007 Loss of imprinting of IGF2 as an epigenetic marker for the risk of human cancer. *Disease Markers* **23** 105–112. (<https://doi.org/10.1155/2007/363464>)
- Dasari A, Shen C, Halperin D, Zhao B, Zhou S, Xu Y, Shih T & Yao JC 2017 Trends in the incidence, prevalence, and survival outcomes in patients with neuroendocrine tumors in the United States. *JAMA Oncology* **3** 1335–1342. (<https://doi.org/10.1001/jamaoncol.2017.0589>)
- Dejeux E, Olaso R, Dousset B, Audebourg A, Gut IG, Terris B & Tost J 2009 Hypermethylation of the IGF2 differentially methylated region 2 is a specific event in insulinomas leading to loss-of-imprinting and overexpression. *Endocrine-Related Cancer* **16** 939–952. (<https://doi.org/10.1677/ERC-08-0331>)
- DePristo MA, Banks E, Poplin R, Garimella KV, Maguire JR, Hartl C, Philippakis AA, del Angel G, Rivas MA, Hanna M, *et al.* 2011 A framework for variation discovery and genotyping using next-generation DNA sequencing data. *Nature Genetics* **43** 491–498. (<https://doi.org/10.1038/ng.806>)
- Du YC, Lewis BC, Hanahan D & Varmus H 2007 Assessing tumor progression factors by somatic gene transfer into a mouse model: Bcl-xL promotes islet tumor cell invasion. *PLoS Biology* **5** e276. (<https://doi.org/10.1371/journal.pbio.0050276>)
- Du Y, Ter-Minassian M, Brais L, Brooks N, Waldron A, Chan JA, Lin X, Kraft P, Christiani DC & Kulke MH 2016 Genetic associations with neuroendocrine tumor risk: results from a genome-wide association study. *Endocrine-Related Cancer* **23** 587–594. (<https://doi.org/10.1530/ERC-16-0171>)
- Dumanski JP, Rasi C, Bjorklund P, Davies H, Ali AS, Gronberg M, Welin S, Sorbye H, Gronbaek H, Cunningham JL, *et al.* 2017 A MUTYH germline mutation is associated with small intestinal neuroendocrine tumors. *Endocrine-Related Cancer* **24** 427–443. (<https://doi.org/10.1530/ERC-17-0196>)
- Francis JM, Kiezun A, Ramos AH, Serra S, Pedamallu CS, Qian ZR, Banck MS, Kanwar R, Kulkarni AA, Karpathakis A, *et al.* 2013 Somatic mutation of CDKN1B in small intestine neuroendocrine tumors. *Nature Genetics* **45** 1483–1486. (<https://doi.org/10.1038/ng.2821>)
- Gangi A, Siegel E, Barmparas G, Lo S, Jamil LH, Hendifar A, Nissen NN, Wolin EM & Amersi F 2018 Multifocality in small bowel neuroendocrine tumors. *Journal of Gastrointestinal Surgery* **22** 303–309. (<https://doi.org/10.1007/s11605-017-3586-8>)
- Grant SG, Seidman I, Hanahan D & Bautch VL 1991 Early invasiveness characterizes metastatic carcinoid tumors in transgenic mice. *Cancer Research* **51** 4917–4923.
- Halperin DM, Shen C, Dasari A, Xu Y, Chu Y, Zhou S, Shih YT & Yao JC 2017 Frequency of carcinoid syndrome at neuroendocrine tumour diagnosis: a population-based study. *Lancet: Oncology* **18** 525–534. ([https://doi.org/10.1016/S1470-2045\(17\)30110-9](https://doi.org/10.1016/S1470-2045(17)30110-9))
- Hanahan D 1985 Heritable formation of pancreatic beta-cell tumours in transgenic mice expressing recombinant insulin/simian virus 40 oncogenes. *Nature* **315** 115–122. (<https://doi.org/10.1038/315115a0>)
- Henfling M, Perren A, Schmitt AM, Saddig CM, Starke AA, Riedl RG, Versleijen-Jonkers YMH, Sprij-Mooij DM, Ramaekers FCS, Hofland L, *et al.* 2018 The IGF pathway is activated in insulinomas but downregulated in metastatic disease. *Endocrine-Related Cancer* **25** 1005–1018. (<https://doi.org/10.1530/ERC-18-0222>)
- Jiao Y, Shi C, Edil BH, de Wilde RF, Klimstra DS, Maitra A, Schulick RD, Tang LH, Wolfgang CL, Choti MA, *et al.* 2011 DAXX/ATRX, MEN1, and mTOR pathway genes are frequently altered in pancreatic neuroendocrine tumors. *Science* **331** 1199–1203. (<https://doi.org/10.1126/science.1200609>)
- Kajimura S, Aida K & Duan C 2005 Insulin-like growth factor-binding protein-1 (IGFBP-1) mediates hypoxia-induced embryonic growth and developmental retardation. *PNAS* **102** 1240–1245. (<https://doi.org/10.1073/pnas.0407443102>)
- Kamilaris CDC & Stratakis CA 2019 Multiple endocrine neoplasia Type 1 (MEN1): an update and the significance of early genetic and clinical diagnosis. *Frontiers in Endocrinology* **10** 339. (<https://doi.org/10.3389/fendo.2019.00339>)
- Katona TM, Jones TD, Wang M, Abdul-Karim FW, Cummings OW & Cheng L 2006 Molecular evidence for independent origin of multifocal neuroendocrine tumors of the enteropancreatic axis. *Cancer Research* **66** 4936–4942. (<https://doi.org/10.1158/0008-5472.CAN-05-4184>)
- Kobayashi S, Contractor T, Vosburgh E, Du YN, Tang LH, Clausen R & Harris CR 2019 Alleles of Insm1 determine whether RIP1-Tag2 mice produce insulinomas or nonfunctioning pancreatic neuroendocrine tumors. *Oncogenesis* **8** 16. (<https://doi.org/10.1038/s41389-019-0127-1>)
- Kolby L, Bernhardt P, Ahlman H, Wangberg B, Johanson V, Wigander A, Forsell-Aronsson E, Karlsson S, Ahren B, Stenman G, *et al.* 2001 A transplantable human carcinoid as model for somatostatin receptor-mediated and amine transporter-mediated radionuclide uptake. *American Journal of Pathology* **158** 745–755. ([https://doi.org/10.1016/S0002-9440\(10\)64017-5](https://doi.org/10.1016/S0002-9440(10)64017-5))
- Leick MB, Shoff CJ, Wang EC, Congress JL & Gallicano GI 2012 Loss of imprinting of IGF2 and the epigenetic progenitor model of cancer. *American Journal of Stem Cells* **1** 59–74.
- Li H & Durbin R 2009 Fast and accurate short read alignment with Burrows-Wheeler transform. *Bioinformatics* **25** 1754–1760. (<https://doi.org/10.1093/bioinformatics/btp324>)
- Massague J 2012 TGFbeta signalling in context. *Nature Reviews: Molecular Cell Biology* **13** 616–630. (<https://doi.org/10.1038/nrm3434>)
- Maxwell JE, Sherman SK, Li G, Choi AB, Bellizzi AM, O'Dorisio TM & Howe JR 2015 Somatic alterations of CDKN1B are associated with small bowel neuroendocrine tumors. *Cancer Genetics* **208** 564–570. (<https://doi.org/10.1016/j.cancergen.2015.08.003>)
- Miao R, Luo H, Zhou H, Li G, Bu D, Yang X, Zhao X, Zhang H, Liu S, Zhong Y, *et al.* 2014 Identification of prognostic biomarkers in hepatitis B virus-related hepatocellular carcinoma and stratification by integrative multi-omics analysis. *Journal of Hepatology* **61** 840–849. (<https://doi.org/10.1016/j.jhep.2014.05.025>)
- Modlin IM, Lye KD & Kidd M 2003 A 5-decade analysis of 13,715 carcinoid tumors. *Cancer* **97** 934–959. (<https://doi.org/10.1002/cncr.11105>)
- Neklason DW, VanDerslice J, Curtin K & Cannon-Albright LA 2016 Evidence for a heritable contribution to neuroendocrine tumors of the small intestine. *Endocrine-Related Cancer* **23** 93–100. (<https://doi.org/10.1530/ERC-15-0442>)
- Pfagner R, Wirnsberger G, Niederle B, Behmel A, Rinner I, Mandl A, Wawrina E, Luo J, Adamiker D, Hoger H, *et al.* 1996 Establishment of a continuous cell line from a human carcinoid of the small intestine (KRJ-I). *International Journal of Oncology* **8** 513–520. (<https://doi.org/10.3892/ijo.8.3.513>)
- Pfagner R, Behmel A, Hoger H, Beham A, Ingolic E, Stelzer I, Svejda B, Moser VA, Obenauf AC, Siegl V, *et al.* 2009 Establishment and characterization of three novel cell lines - P-ST5, L-ST5, H-ST5 - derived from a human metastatic midgut carcinoid. *Anticancer Research* **29** 1951–1961.
- Scarpa A 2019 The landscape of molecular alterations in pancreatic and small intestinal neuroendocrine tumours. *Annales d'Endocrinologie* **80** 153–158. (<https://doi.org/10.1016/j.ando.2019.04.010>)

- Sei Y, Zhao X, Forbes J, Szymczak S, Li Q, Trivedi A, Voellinger M, Joy G, Feng J, Whatley M, *et al.* 2015 A hereditary form of small intestinal carcinoid associated With a germline mutation in inositol polyphosphate multikinase. *Gastroenterology* **149** 67–78. (<https://doi.org/10.1053/j.gastro.2015.04.008>)
- Shen HC, He M, Powell A, Adem A, Lorang D, Heller C, Grover AC, Ylaya K, Hewitt SM, Marx SJ, *et al.* 2009 Recapitulation of pancreatic neuroendocrine tumors in human multiple endocrine neoplasia type I syndrome via Pdx1-directed inactivation of Men1. *Cancer Research* **69** 1858–1866. (<https://doi.org/10.1158/0008-5472.CAN-08-3662>)
- Strosberg JR, Halfdanarson TR, Bellizzi AM, Chan JA, Dillon JS, Heaney AP, Kunz PL, O'Dorisio TM, Salem R, Segelov E, *et al.* 2017 The North American Neuroendocrine Tumor Society consensus guidelines for surveillance and medical management of midgut neuroendocrine tumors. *Pancreas* **46** 707–714. (<https://doi.org/10.1097/MPA.0000000000000850>)
- Tran VG, Court F, Duputie A, Antoine E, Aptel N, Milligan L, Carbonell F, Lelay-Taha MN, Piette J, Weber M, *et al.* 2012 H19 antisense RNA can up-regulate Igf2 transcription by activation of a novel promoter in mouse myoblasts. *PLoS ONE* **7** e37923. (<https://doi.org/10.1371/journal.pone.0037923>)
- Wang GG, Yao JC, Worah S, White JA, Luna R, Wu TT, Hamilton SR & Rashid A 2005 Comparison of genetic alterations in neuroendocrine tumors: frequent loss of chromosome 18 in ileal carcinoid tumors. *Modern Pathology* **18** 1079–1087. (<https://doi.org/10.1038/modpathol.3800389>)
- Wells SA, Jr, Pacini F, Robinson BG & Santoro M 2013 Multiple endocrine neoplasia type 2 and familial medullary thyroid carcinoma: an update. *Journal of Clinical Endocrinology and Metabolism* **98** 3149–3164. (<https://doi.org/10.1210/jc.2013-1204>)
- Wong C, Tang LH, Davidson C, Vosburgh E, Chen W, Foran DJ, Notterman DA, Levine AJ & Xu EY 2020 Two well-differentiated pancreatic neuroendocrine tumor mouse models. *Cell Death and Differentiation* **27** 269–283. (<https://doi.org/10.1038/s41418-019-0355-0>)
- Zhao J, de Krijger RR, Meier D, Speel EJ, Saremaslani P, Muletta-Feurer S, Matter C, Roth J, Heitz PU & Komminoth P 2000 Genomic alterations in well-differentiated gastrointestinal and bronchial neuroendocrine tumors (carcinoids): marked differences indicating diversity in molecular pathogenesis. *American Journal of Pathology* **157** 1431–1438. ([https://doi.org/10.1016/S0002-9440\(10\)64780-3](https://doi.org/10.1016/S0002-9440(10)64780-3))

Received in final form 10 January 2020

Accepted 16 January 2020

Accepted Manuscript published online 17 January 2020

ARTICLE

Open Access

Alleles of *Insm1* determine whether RIP1-Tag2 mice produce insulinomas or nonfunctioning pancreatic neuroendocrine tumors

Shinta Kobayashi¹, Tanupriya Contractor², Evan Vosburgh², Yi-Chieh Nancy Du³, Laura H. Tang⁴, Richard Clausen² and Chris R. Harris^{2,5,6}

Abstract

The two most common types of pancreatic neuroendocrine tumors (PanNETs) are insulinomas and nonfunctioning PanNETs (NF-PanNETs). Insulinomas are small, rarely metastatic tumors that secrete high amounts of insulin, and nonfunctioning PanNETs are larger tumors that are frequently metastatic but that do not secrete hormones. Insulinomas are modeled by the highly studied RIP1-Tag2 (RT2) transgenic mice when bred into a C57Bl/6 (B6) genetic background (also known as RT2 B6 mice). But there has been a need for an animal model of nonfunctioning PanNETs, which in the clinic are a more common and severe disease. Here we show that when bred into a hybrid AB6F1 genetic background, RT2 mice make nonfunctioning PanNETs. Compared to insulinomas produced by RT2 B6 mice, the tumors produced by RT2 AB6F1 mice were larger and more metastatic, and the animals did not suffer from hypoglycemia or hyperinsulinemia. Genetic crosses revealed that a locus in mouse chromosome 2qG1 was linked to liver metastasis and to lack of insulin production. This locus was tightly linked to the gene encoding *Insm1*, a beta cell transcription factor that was highly expressed in human insulinomas but unexpressed in other types of PanNETs due to promoter hypermethylation. *Insm1*-deficient human cell lines expressed stem cell markers, were more invasive in vitro, and metastasized at higher rates in vivo when compared to isogenic *Insm1*-expressing cell lines. These data demonstrate that expression of *Insm1* can determine whether a PanNET is a localized insulinoma or a metastatic nonfunctioning tumor.

Introduction

Neuroendocrine cells function by secreting hormones in response to neurological or metabolic stimuli. The insulin-producing beta cells of the pancreas are the best-known example of neuroendocrine cells, because beta cell defects can result in diabetes. Neuroendocrine cells are also found in many other sites of the body, including the pituitary, thyroid, parathyroid, small and large intestine.

In order to maintain proper hormone balance, neuroendocrine cells are under tight growth regulation. However, neuroendocrine cells can become transformed and develop into neuroendocrine tumors. Transformation of pancreatic beta cells results in pancreatic neuroendocrine tumors (PanNETs). PanNETs are the second most common tumors of the pancreas, with an incidence of 1 per 200,000, and the incidence of PanNETs has been increasing rapidly¹. PanNETs often metastasize to the liver.

For such an uncommon disease, PanNETs have been a surprisingly popular research subject for tumor biologists. This is partly due to the fact that PanNETs are produced

Correspondence: Chris R. Harris (harrisch@ca.rutgers.edu)

¹Institute for Advanced Study, Princeton, NJ, USA

²Raymond and Beverly Sackler Foundation Laboratory, New Brunswick, NJ, USA

Full list of author information is available at the end of the article.

These authors contributed equally: Shinta Kobayashi, Tanupriya Contractor

© The Author(s) 2019



Open Access This article is licensed under a Creative Commons Attribution 4.0 International License, which permits use, sharing, adaptation, distribution and reproduction in any medium or format, as long as you give appropriate credit to the original author(s) and the source, provide a link to the Creative Commons license, and indicate if changes were made. The images or other third party material in this article are included in the article's Creative Commons license, unless indicated otherwise in a credit line to the material. If material is not included in the article's Creative Commons license and your intended use is not permitted by statutory regulation or exceeds the permitted use, you will need to obtain permission directly from the copyright holder. To view a copy of this license, visit <http://creativecommons.org/licenses/by/4.0/>.

by the RIP1-Tag2 tumor model (RT2), which was one of the very first transgenic mouse models for cancer². PanNETs occur in RT2 mice due to expression of the SV40 T-antigen oncoprotein (Tag) from a rat insulin promoter (RIP). Tumor formation in RT2 mice is rapid and synchronized, which facilitates the testing of both potential therapeutics and potential tumor genes. RT2 is also a rare example of a mouse model that has been validated pharmacologically. Sunitinib and rapamycin were shown to block growth of tumors in RT2 mice^{3,4}; these drugs were subsequently tested in clinical trials^{5,6}, and approved by the FDA for use in patients. Conversely, antibodies against IGF1 receptor failed to block tumor progression in RT2 mice, and subsequently failed in the clinic^{7,8}. The clinical success of RT2 as a model organism also prompted a reexamination of the Rb pathway in human PanNETs, because Rb is inactivated by the SV40 T-antigen. This analysis led to discovery of Cdk4 and Cdk6 amplifications and high Rb phosphorylation in pancreatic neuroendocrine tumors, as well as the demonstration that PanNET cell lines responded to Cdk4/6 inhibition especially in combination with rapamycin⁹. This study helped lead to a clinical trial of a Cdk4/6 inhibitor in combination with rapamycin-analog everolimus (ClinicalTrials.gov identifier NCT03070301). In another trial, a combination of the VEGFR2 inhibitor sunitinib and the c-met inhibitor PF-04217903 blocked tumor progression in RT2 mice¹⁰; subsequently, a PanNET patient clinical trial was initiated to test the effects of cabozantinib, a single agent targeting both VEGFR2 and c-met¹¹.

The liver metastasis found in patients with PanNETs can also be detected in RT2 mice, although the frequency of metastasis is generally low. Researchers have published many reports on genes that can increase the rate of metastasis in this mouse, including *Igf1r*, *Alk*, *Rhamm*, *Met*, *Bclx*, and *C5* (refs. 10,12–16). Also, *Csfl* has been shown to be a metastasis suppressor in RT2 mice¹⁷.

Clinically, metastasis correlates with whether or not PanNETs produce insulin. PanNETs producing insulin are called insulinomas and these tumors are rarely malignant or metastatic; conversely, non-insulin-producing PanNETs are often highly malignant and metastatic¹⁸. Most of the non-insulin-producing PanNETs are “nonfunctioning” tumors (NF-PanNETs), so-named because they do not overproduce any of the major pancreatic endocrine hormones¹⁸. NF-PanNETs are by far the most clinically important of the pancreatic neuroendocrine tumors. It has been estimated that about 85% of PanNETs are nonfunctioning, 10% are insulinomas, and the remaining tumors express other hormones such as gastrin or glucagon¹⁹. Patients with nonfunctioning PanNETs have a 5-year survival rate of only 33%¹⁹, whereas patients with insulinomas rarely die of their

disease. Nonfunctioning tumors are also larger in size than insulinomas.

Here we demonstrate that the RT2 mouse model is capable of modeling both insulinomas and nonfunctioning PanNETs, with the specific disease dependent on the genetic background of the animals. In a hybrid AB6F1 genetic background, low expression levels of a beta cell transcription factor, *Insm1*, favors development of nonfunctioning tumors, whereas in a C57Bl/6 genetic background, higher expression of *Insm1* favors development of insulinomas. Amounts of *Insm1* correlated with insulin production and with lack of metastasis, in both mice and patients.

Results

RT2 AB6F1 mice were generated by mating females from the inbred A/J genetic background to male RT2 B6 mice, which have an inbred C57Bl/6 J genetic background¹². For both genetic backgrounds, pancreatic tumors were produced that were neuroendocrine tumors upon pathological examination, albeit less well-differentiated than the PanNETs found in most patients. There was a difference in frequency of liver metastasis in the two genetic backgrounds, with metastasis being much more common in RT2 AB6F1 mice than in RT2 B6 mice (Fig. 1a). Other genetic backgrounds have also been reported to influence metastasis frequency of RT2 mice¹³. Primary tumors were larger in age-matched RT2 AB6F1 mice compared to RT2 B6 (Fig. 1b). For RT2 AB6F1 animals, tumor size correlated with the presence of metastasis (Supplemental Fig. 1), while for RT2 B6 animals, a correlation between metastasis and tumor size was not tested because there were so few cases of animals with metastasis.

Remarkably, in spite of having larger, more metastatic tumors, RT2 AB6F1 mice actually lived longer than RT2 B6 mice (Fig. 1c). Eighty-five percent of RT2 AB6F1 mice but only 33% of RT2 B6 mice lived to an age of 16 weeks. Early mortality may be related to hypoglycemia, which could be observed only in RT2 B6 mice and not in RT2 AB6F1 mice (Fig. 1d). Hypoglycemia has previously been reported in RT2 mice, so it was actually a surprise to find out that the RT2 AB6F1 were not hypoglycemic. In keeping with their hypoglycemia, RT2 B6 mice were also severely hyperinsulinemic, with an average nine-fold increase in serum insulin compared to wildtype B6 mice (Fig. 1e). Conversely, in spite of their larger pancreatic neuroendocrine tumors, RT2 AB6F1 expressed only two-fold more serum insulin than wildtype AB6F1 mice. Immunohistochemistry revealed robust staining for insulin in tumors from RT2 B6 animals, but no insulin staining in tumors from RT2 AB6F1 animals (Supplemental Fig. 2).

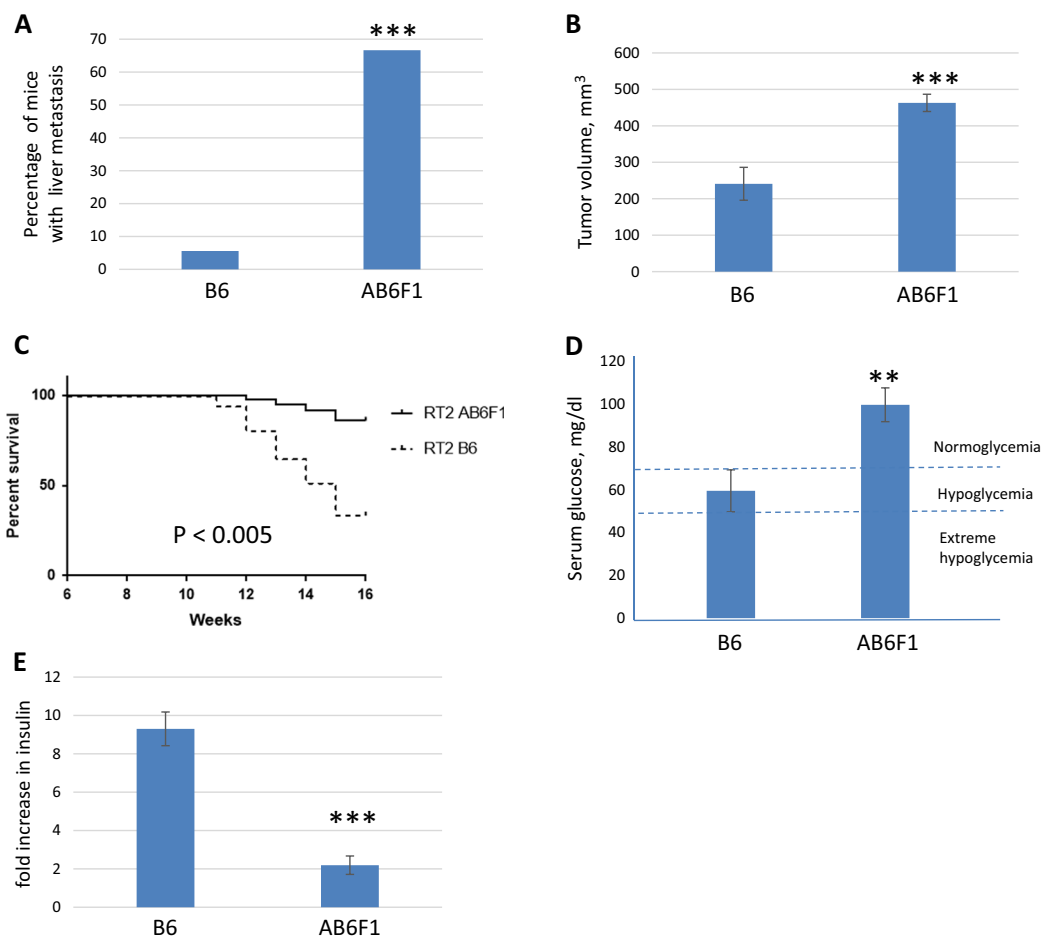


Fig. 1 RT2 B6 and RT2 AB6F1 mice show profound phenotypic differences. **a** Percentage of 15-week-old RT2 mice with liver metastasis, by genetic background. All mice were males, and 18 mice from each lineage were analyzed. Statistical significance was determined using Fisher's exact test. B6 mice have the C57Bl/6 genetic background, and AB6F1 mice are hybrids resulting from mating female A/J mice to male C57Bl/6 mice. **b** Volume of primary pancreatic tumors according to the genetic background. All mice were 17-week-old males; 24 RT2 B6 mice and 138 RT2 AB6F1 mice were analyzed. Statistical significance was determined using Mann–Whitney test. **c** Kaplan–Meier survival curves for RT2 mice between 6 and 16 weeks of age according to the genetic background. **d** Eight hours after removal of food, serum glucose was measured in RT2 mice of different genetic backgrounds. All mice were males and 12–13 weeks old. Fifteen RT2 AB6F1 and 12 RT2 B6 were analyzed. Statistical significance was determined using two-tailed *t*-test. **e** RT2 mice or wildtype littermates were held without food for 8 h, then serum insulin was measured and compared to littermates (B6 or AB6F1) lacking the SV40 T-antigen transgene. Mice were males and 13 weeks old. Nine and 11 RT2 B6 and RT2 AB6F1 mice were measured, respectively. Statistical significance was determined using two-tailed *t*-test

Primary pancreatic tumors from both RT2 B6 and RT2 AB6F1 mice were harvested, and the latter expressed lower levels of mRNA for insulin (Fig. 2a), consistent with the low levels of serum insulin in these animals. Tumors from RT2 AB6F1 mice also transcribed less mRNA for other beta cell markers such as *MafA*, *Pdx1*, and *Nkx6-1* (Fig. 2a). Interestingly, transcription of the gene for SV40 T-antigen did not differ between tumors from RT2 AB6F1 and RT2 B6 mice (Fig. 2b), even though insulin expression differs strongly between the two mice. This may reflect the leakiness of the RIP that controls expression of SV40 T-antigen; this transgene has also been shown to express

in other insulin-negative neuroendocrine cells from small intestine and pituitary^{20,21}.

With their smaller tumors, low metastasis, hypoglycemia, and hyperinsulinemia, RT2 B6 mice have all of the clinical features of human insulinomas. RT2 AB6F1 mice, on the other hand, may develop some other kind of pancreatic neuroendocrine tumor that does not express insulin. In RT2 AB6F1 tumors, transcription of glucagon and vasoactive intestinal peptide were not elevated, transcription of PPY and gastrin decreased, but transcription of somatostatin increased (Fig. 2c). Although elevated, the levels of somatostatin transcription were still

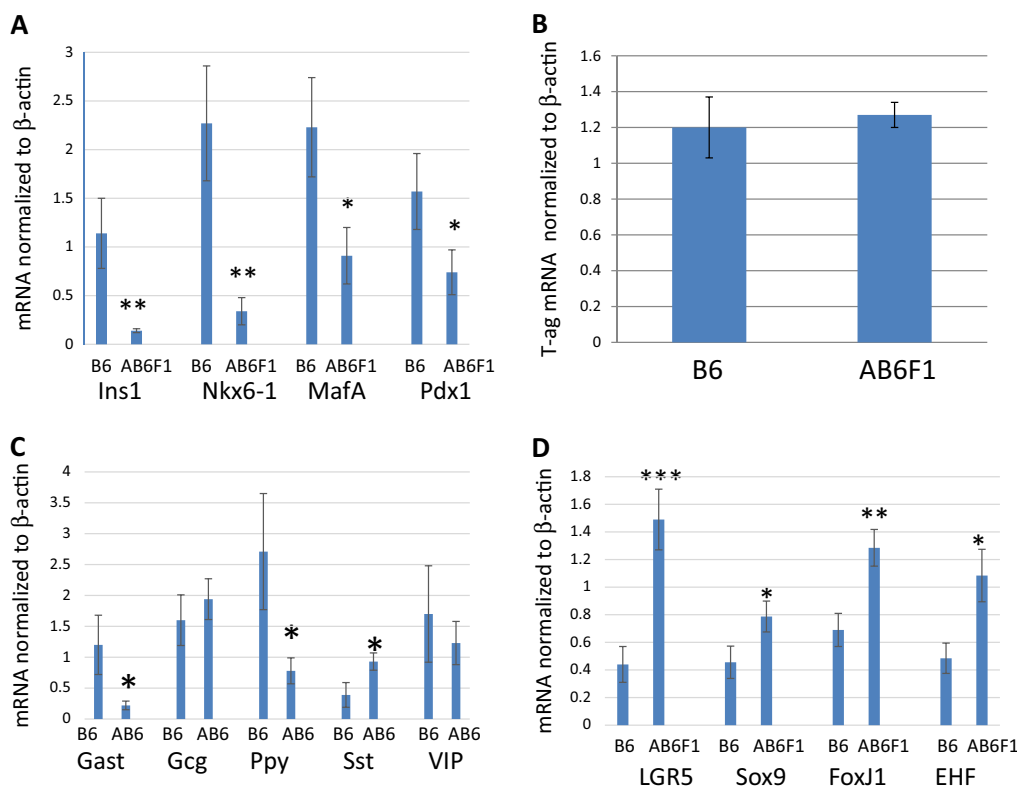


Fig. 2 Tumors from RT2 AB6F1 mice profile as nonfunctioning pancreatic neuroendocrine tumors. In each figure, Q-PCR was used to measure gene expression, using cDNA prepared from primary tumors isolated from 17 male RT2 B6 mice and from 25 male RT2 AB6F1 mice. All statistical analysis was performed using two-tailed *t*-test. **a** Beta cell markers insulin-1 (*Ins1*), *Nkx6-1*, *MafA*, and *Pdx1*. **b** SV40 T-antigen, which is the oncogene that drives tumorigenesis in RT2 mice. **c** Pancreatic neuroendocrine hormones gastrin (*Gast*), glucagon (*Gcg*), pancreatic polypeptide (*Ppy*), somatostatin (*Sst*), and vasoactive intestinal peptide (*Vip*). **d** Pancreatic stem cell markers *Lgr5*, *Sox9*, *FoxJ1*, and *EHF*

low. Patients with somatostatinomas suffer from weight loss and diarrhea, whereas RT2 AB6F1 were slightly overweight and had firm stools (data not shown). From these experiments, we conclude that tumors produced by RT2 AB6F1 mice profiled as nonfunctioning PanNETs, a clinically important disease in which patient tumors do not express high levels of any of the pancreatic hormones.

Thus in spite of sharing 50% genetic identity, RT2 AB6F1 and RT2 B6 mice develop two very different types of PanNET. A possible clue for the genetic basis of this difference came from analysis of transcription of several markers of pancreatic stem cells²², which increased in tumors from RT2 AB6F1 mice (Fig. 2d). The loss of differentiation (Fig. 2a) but gain in stem cell markers (Fig. 2d) in RT2 AB6F1 tumors led to a hypothesis that A/J and B6 mice may have different allelic forms of some beta cell differentiation factor.

Among the many genes known to be important for beta cell differentiation is *Insm1*, which can drive transdifferentiation of pancreatic ductal cells to endocrine cells²³, presumably through a stem cell intermediate. *Insm1*-knockout mice have also been reported to make beta cells

that are deficient in expression of insulin²⁴, which is perhaps similar to the deficient expression of insulin in tumors of RT2 AB6F1 mice. Notably, *Insm1* was first isolated as a very highly expressed RNA in insulinomas²⁵.

As shown in Fig. 3a, expression of *Insm1* mRNA was higher in the insulinomas from RT2 B6 and lower in nonfunctioning tumors from RT2 AB6F1 mice. *Insm1* protein levels were also higher in tumors from RT2 B6, as shown by western blotting (Fig. 3b). These experiments suggested that *Insm1* might be relevant to the insulinomas and to the nonfunctioning tumors observed in RT2 mice.

Insm1 expression was characterized within a large set of patient samples. As shown in Fig. 3c, the mRNA of *Insm1* strongly correlated with the mRNA of insulin. DNA was prepared from 16 of these human tumors, 8 of which expressed high amounts of insulin and 8 of which expressed very little insulin. Tumor DNAs were treated with bisulfite, and methylation-specific PCR was performed to test for DNA methylation within the promoter region of the *Insm1* gene. As shown in Fig. 3d, the *Insm1* promoter was more strongly methylated in the tumors with low insulin and low *Insm1*. Since promoter

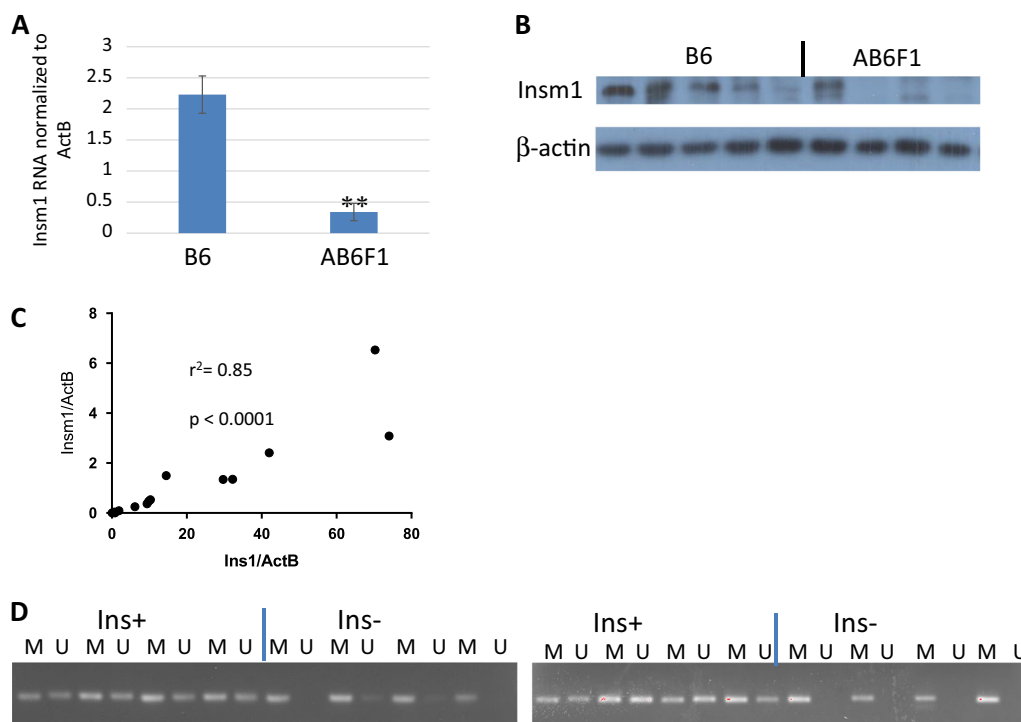


Fig. 3 Insulinomas from humans and mice express high levels of transcription factor *Insm1*. **a** Q-PCR analysis of *Insm1* expression from primary tumors isolated from 17 male RT2 B6 mice or from 25 male RT2 AB6F1 mice. Statistical significance was determined using two-tailed *t*-test. **b** Western blot analyses of *Insm1* and β -actin expression from pancreatic neuroendocrine tumors of RT2 B6 or RT2 AB6F1 mice. **c** mRNA and cDNA were prepared from 39 human pancreatic neuroendocrine tumors, and transcription of beta cell markers *Ins1* and *Insm1* was assayed by Q-PCR. Most of the tumors occupy the (0,0) point of the graph. Statistical analysis was performed by Pearson correlation. **d** Tumor DNA from 16 patients was subjected to bisulfite treatment, followed by PCR using primers directed against a CpG island immediately upstream of the *Insm1* transcription start site. The results of PCR by Methylation-specific primer pairs are shown in lanes marked "M", and results of PCR by Unmethylation-specific primer pairs are shown in the lanes marked "U". In both gels, the first four tumors had high insulin expression by Q-PCR analysis, and the second four tumors had undetectable insulin expression by Q-PCR analysis. Tumors were arbitrarily defined as having high insulin expression if they had an *Insm1/ActB* mRNA ratio above 1.0 (see **c**). The eight insulin-negative tumors are likely to be nonfunctioning tumors, given the fact that 85% of PanNETs are nonfunctioning and 10% of PanNETs express insulin¹⁹. These eight insulin-negative tumors also had low expression of mRNA for gastrin and glucagon (data not shown)

hypermethylation is a common mechanism for lowering expression of key tumor suppressor genes, these data suggest that *Insm1* expression may not merely correlate with insulinomas, but may actually be a gene that suppresses the formation of nonfunctioning PanNETs.

Next we tested whether allelic differences in the *Insm1* genes encoded by the B6 and A/J lineages might be responsible for the insulinomas and NF-PNETs observed in RT2 B6 and RT2 AB6F1 mice, respectively. *Insm1* genotypes were tested in a set of 279 RT2 AB6F2 mice, which had been prepared for a previous study¹². RT2 AB6F2 are the product of mating RT2 AB6F1 mice. Unlike their hybrid F1 parents, which are genetically identical, F2 mice have a 1:2:1 Mendelian ratio of genotypes at all loci: one quarter of offspring will be homozygous for a given gene encoded by the A/J lineage, one quarter will be homozygous for the same gene encoded by the B6 lineage, and one half will be heterozygous at the

locus. If a particular gene from the A/J genetic background promotes metastasis, then homozygotes and possibly heterozygotes for the A/J allele of that gene should be more likely to show liver metastasis. A known SNP difference between the *Insm1* alleles from C57Bl/6 and A/J mice was assayed.

As shown in Fig. 4a, the *Insm1* SNP from the A/J background linked to metastasis in RT2 AB6F2 mice. Particularly notable is the fact that there was more metastasis in heterozygous mice compared to mice homozygous for the B6 allele of *Insm1*; this result matches with the fact that metastasis is more common in RT2 AB6F1 mice, which are heterozygous, than in RT2 B6 mice, which are homozygous for the B6 allele.

Importantly, if the differences in *Insm1* alleles are responsible for the different types of PanNETs, then the *Insm1* allele that links to metastasis should also link to lower insulin production. This is indeed the case. As

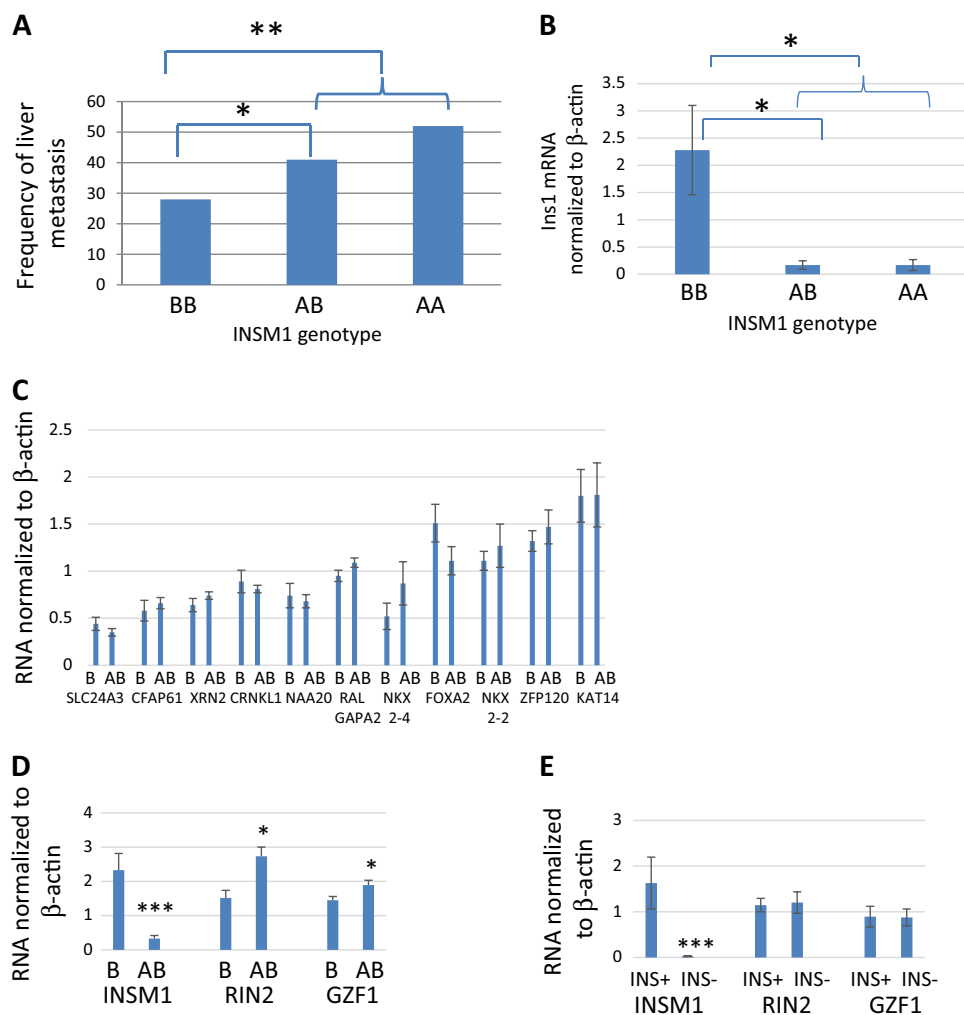
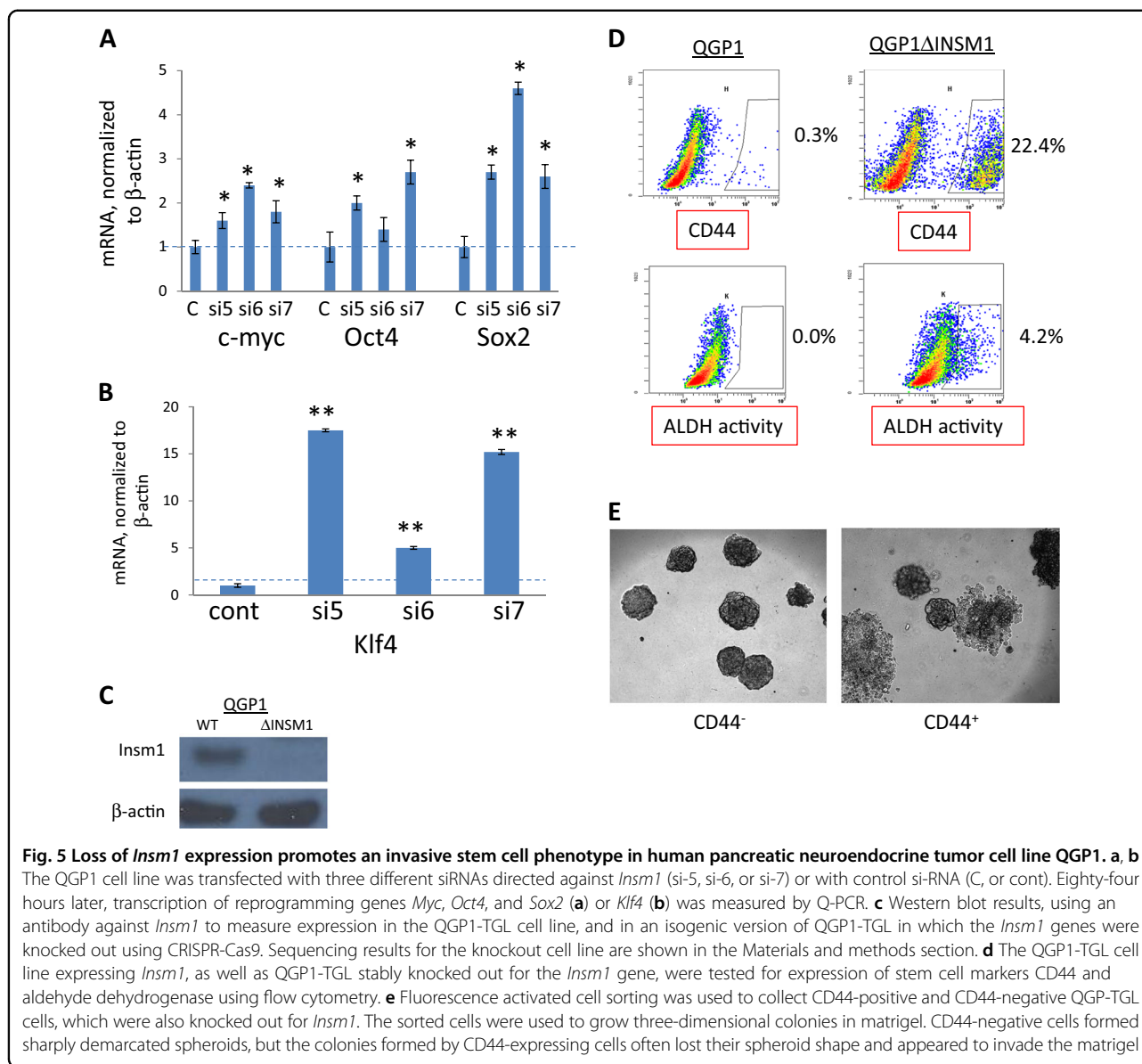


Fig. 4 The *Insm1* locus links to key phenotypic differences between RT2 B6 and RT2 AB6F1 mice. **a** RT2 AB6F2 mice were genotyped for a nucleotide difference within the *Insm1* gene. Animals with two copies of the allele from the A/J lineage are called “AA”, animals with two copies of the allele from the B6 lineage are called “BB,” and heterozygous animals are called “AB”. The mice were also scored for the presence of liver metastasis. A total of 279 mice were assayed. Statistical significance was computed using Fisher’s exact test. **b** Transcription of insulin-1 (*Ins1*) by 37 primary PanNETs from RT2 AB6F2 mice was compared using Q-PCR. The tumors were also genotyped to determine the *Insm1* genotype. Tumors with two *Insm1* alleles from the B6 lineage are denoted “BB,” tumors from heterozygous mice are denoted “AB,” and tumors with two *Insm1* alleles from the A/J lineage are denoted as “AA”. Statistical significance was determined using two-tailed *t*-test. **c** Q-PCR was used to analyze transcription of genes linked to *Insm1* in primary PanNETs from 18 RT2 B6 males and from 24 RT2 AB6F1 males. The total size of the region was 8 MeB, with *Insm1* in the center. All genes within 2 MeB on either side of *Insm1* were assayed, as well as a select number of candidate genes within 4 MeB on either side of *Insm1*. Candidate genes were selected as genes that were known to encode transcription factors and differentiation factors. “B” refers to tumors from RT2 B6 mice and “AB” refers to tumors from RT2 AB6F1 mice. mRNA for several genes within this region, including *OvoL2*, *Kiz*, and *Pax1*, could not be detected in spite of using two separate assays for each gene. **d** Transcription of *Insm1*, *Rin2*, and *GZF1* in primary tumors from 18 RT2 B6 males and from 24 RT2 AB6F1 males was determined using Q-PCR. **e** Transcription of *Insm1*, *Rin2*, and *GZF1* was determined for 39 primary patient pancreatic NETs. Tumors were arbitrarily defined as expressing insulin or not expressing insulin based on *Ins1*/ActB mRNA ratios above or below 1.0, respectively (see Fig. 3c)

shown in Fig. 4b, tumors from heterozygous animals expressed lower levels of mRNA for insulin than tumors from animals that inherited both of their *Insm1* alleles from the B6 lineage. Again, this matches with the lower levels of insulin produced by RT2 AB6F1 mice, which are heterozygous, and with the higher levels of insulin produced by RT2 B6 mice, which are homozygous for the B6

allele. Thus, in F2 animals with at least one copy of *Insm1* from the A/J lineage, there was elevated metastasis and weak expression of insulin when compared to animals with two copies of *Insm1* from the B6 lineage.

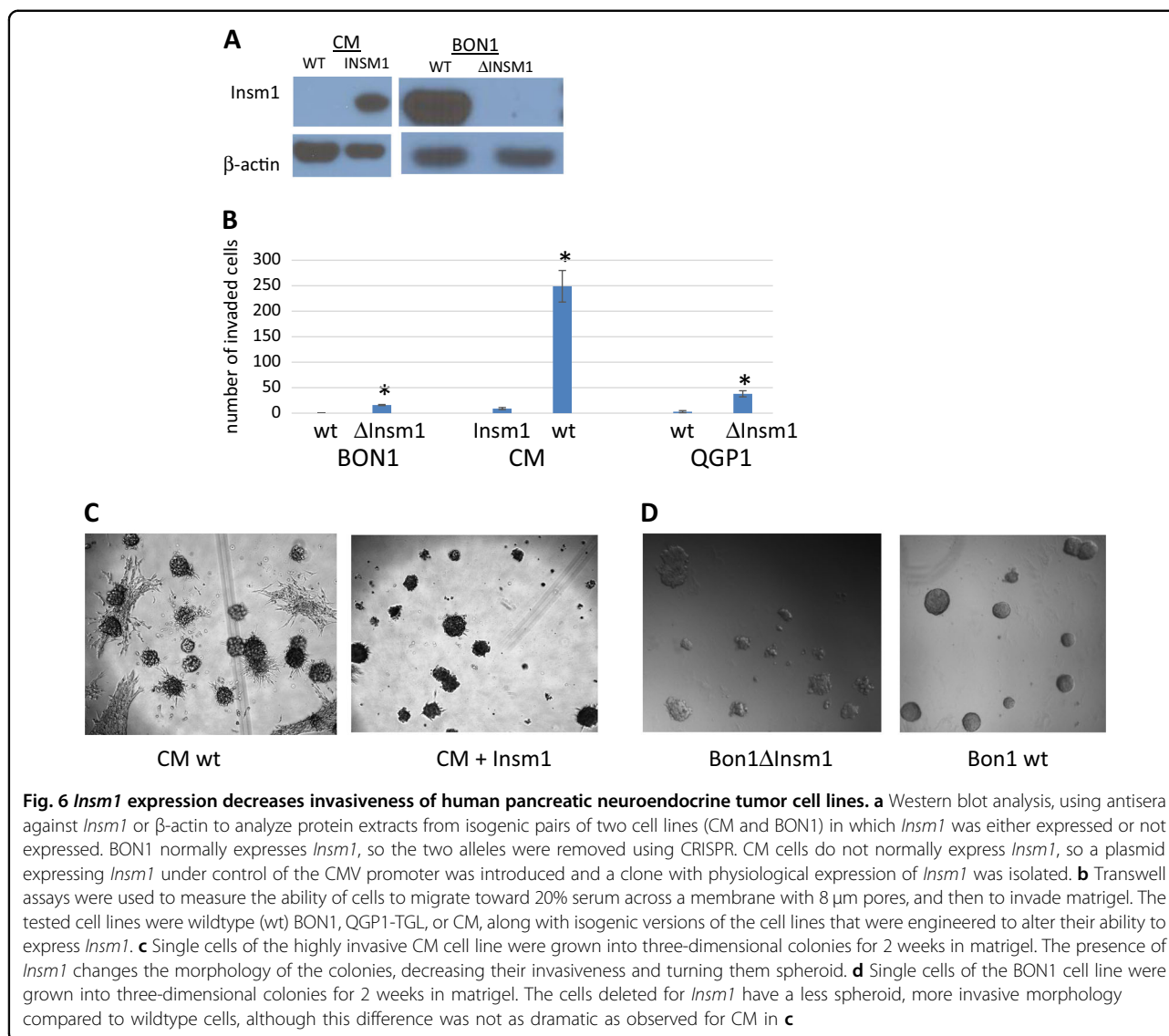
We also considered the possibility that a gene linked to *Insm1*, and not *Insm1* itself, is the actual effector of tumor type in RT2 mice. If true, then perhaps such a gene would



show expression differences in RT2 B6 and RT2 AB6F1 tumors. Among genes residing within an 8 MeB region of the mouse genome, centered at *Insm1*, three genes did show differences in expression between tumors from RT2 B6 and RT2 AB6F1 mice (Fig. 4c, d). However, of these three genes, only *Insm1* expression also showed differences in patient samples expressing high or low levels of insulin (Fig. 4e). Although this study does not completely rule out the possibility that another gene is involved, *Insm1* does appear to be the best candidate.

If alleles of *Insm1* are indeed responsible for the two tumor subtypes, then *Insm1* should be capable of blocking metastasis and dedifferentiation in neuroendocrine tumor cell lines. In Fig. 5a, b, the effect of transient knockdown of *Insm1* expression using three different shRNAs was

tested in the QGP1 cell line. *Insm1* knockdown increased expression of the so-called Yamanaka factors²⁶, which are known to increase pluripotency of differentiated cells. Next, CRISPR-Cas9 technology was used to stably knock out *Insm1* from QGP1-TGL cells, a version of QGP1 engineered to express firefly luciferase (Fig. 5c). The *Insm1* knockout increased the number of cells expressing aldehyde dehydrogenase and CD44, which are markers of stem cells (Fig. 5d). *Insm1*-null QGP1-TGL cells were then sorted for CD44 expression using flow cytometry. CD44-negative QGP1-TGL Δ *Insm1* cells gave rise to spheroid colonies, whereas CD44-positive QGP1-TGL Δ *Insm1* cells produced colonies with invasive morphologies (Fig. 5e). These data indicate that loss of *Insm1* can produce more invasive, stem-like cells.



CRISPR-Cas9 was also used to knock out expression of *Insm1* from a second *Insm1*-expressing PanNET cell line, BON1 (Fig. 6a). We also introduced *Insm1* expression to the CM cell line, a highly undifferentiated PanNET cell line that did not normally express *Insm1* protein (Fig. 6a). Along with QGP1-TGL, each of these isogenic pairs of *Insm1*-expressing and *Insm1*-null cell lines was tested for in vitro invasiveness, using a transwell assay. Invasiveness is a common property of metastatic cells. For all of the cell lines, invasiveness was higher if expression of *Insm1* was absent, indicating that *Insm1* is a repressor of invasion (Fig. 6b). The CM cell line was particularly invasive; the effects of *Insm1* on this cell line could also be seen in three-dimensional culture, in which wildtype CM cells invade the surrounding matrix, but CM cells expressing *Insm1* only form less invasive spheroids (Fig. 6c). Though less dramatic, *Insm1* also has an effect on the morphology

of the BON1 cell line when grown in three-dimensional culture (Fig. 6d); the smaller change in morphology of BON1 correlated with the lower level of invasiveness of BON1 cells compared to CM cells.

Isogenic, *Insm1*-expressing, or *Insm1*-null QGP1-TGL cells were injected into the left ventricles of immune compromised mice. Mice were imaged weekly for bioluminescence of luciferase in order to assay for metastatic spread. Within 2 weeks, strong luciferase signals were detected in the torso, and these were particularly intense in animals injected with *Insm1*-null QGP1 (Fig. 7a). Luciferase signals also occurred above the neck; magnetic resonance imaging of the head revealed unusual growth of cells in the pre-nasal sinuses. Dissection of animals revealed that metastatic lesions were most prominent in the lung, liver, and pancreas. Examples are shown in Fig. 7b, where one of three animals injected with wildtype

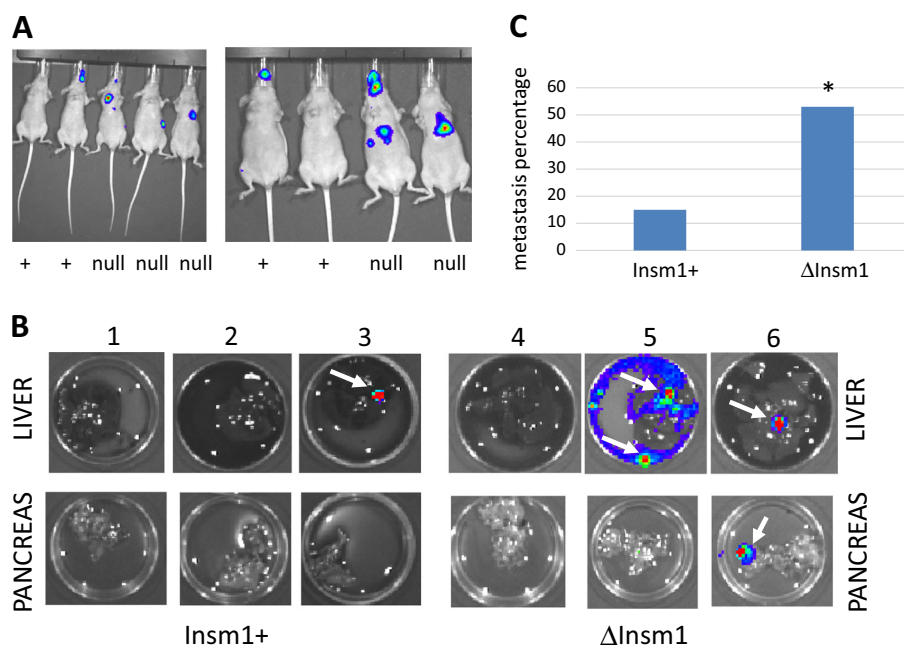


Fig. 7 *Insm1* blocks in vivo metastasis by the QGP1-TGL cell line. **a** The QGP1 cell line was engineered to express firefly luciferase, and isogenic pairs either expressing *Insm1*, or knocked out for *Insm1*, were injected into the left ventricles of nude mice. Three weeks later, metastatic lesions were imaged in live mice following injection of luciferin. In both photos, the two mice on the left were injected with cells that express *Insm1* (+), and the other animals were injected with cells unable to express *Insm1* (null). **b** Three weeks after intracardial injection of luciferase-expressing QGP1 cells, mice were euthanized, and pancreas and liver were removed and treated with luciferin to help image metastases. The first three mice were injected with *Insm1*-expressing QGP1, and mice 4, 5, and 6 were injected with *Insm1*-negative QGP1. Livers are in the upper row and pancreases are in the lower row. Metastases are noted by arrow. **c** Quantitation of metastases from lung, pancreas, and liver, which were isolated from 14 mice treated with luciferase-expressing QGP-TGL cells that either express or cannot express *Insm1*. Metastasis was arbitrarily defined as individual organs giving radiance readings above 10^5 photons/s/cm²/steradian following luciferin treatment. Statistical significance was determined using Fisher's exact test

QGP-TGL produced a small lesion in the liver (animal number 3), but two of three animals (animals 5 and 6) injected with QGP-TGL knocked out for *Insm1* produced lesions in the pancreas and in the liver. Altogether, the presence of metastatic tumors was 3.3-fold more common in the animals injected with the cell line knocked out for *Insm1* (Fig. 7c).

Together, these cell line experiments establish that depletion of *Insm1* can cause stem-like cells to form, can increase invasiveness, and can cause metastasis; furthermore, these data suggest that the difference between the less metastatic, more differentiated insulinomas of RT2 B6 mice and the NF-PanNETs of RT2 AB6F1 mice may be due to differences in *Insm1* expression. Coupled with the genetic linkage experiments from RT2 AB6F2 mice, the cell line data strongly suggest that allelic differences in *Insm1* between the A/J and B6 mouse lines lead to different types of neuroendocrine tumors in RT2 mice.

Discussion

In two different genetic backgrounds (B6 and AB6F1), RT2 mice produced different types of PanNETs:

insulinomas and nonfunctioning PanNETs, respectively. Several lines of evidence supported the idea that allelic differences in the *Insm1* gene were responsible for the difference in tumor types, and that *Insm1* is a suppressor gene of nonfunctioning PanNETs. First and most importantly, in RT2 AB6F2 mice, the *Insm1* locus linked strongly to high metastasis and to low insulin expression, which are two key characteristics of NF-PanNETs. Second, *Insm1* expression was lower in NF-PanNETs, compared to insulinomas. Third, the *Insm1* promoter was hypermethylated in human NF-PanNETs, as is often observed for tumor suppressor genes. Fourth, a key feature of NF-PanNETs is metastasis, and knockout of *Insm1* was sufficient to increase in vivo metastasis of a pancreatic neuroendocrine cell line, QGP1-TGL1, and to increase in vitro invasiveness of additional neuroendocrine cell lines.

Insm1 is a transcription factor that promotes beta cell differentiation²⁷, and other tissue-specific differentiation factors have also been shown to suppress metastasis, such as GATA3 in breast tumors²⁸ and NKX2-1 in lung tumors²⁹. It is generally thought that loss of these differentiation factors leads to metastasis by causing

dedifferentiation to stem cells, and that stem cells increase metastasis because they are more invasive and less prone to anoikis^{30–32}. Expression of stem cell markers increased in low *Insm1*-expressing tumors from RT2 AB6F1 mice (Fig. 2d). Upon knockout of *Insm1* in the QGP1 cell line, stem cell markers increased, invasiveness increased, and metastasis increased.

The A/J and B6 lineages show several nucleotide differences within and near the *Insm1* locus, and it is possible that one or more of these differences affect *Insm1* transcription or RNA stability. It is also formally possible that the *Insm1* alleles in these lineages are not different at all and that another gene, linked to *Insm1*, can affect *Insm1* expression. But we detected no evidence for such a mechanism, such as differential expression of another linked gene.

Interestingly, *Insm1* is not the only allelic difference between the B6 and A/J lineages that affects neuroendocrine tumors. In our initial study of RT2 AB6F2 mice, we showed that the A/J genome harbored a recessive, metastasis-suppressing locus, due to an inactivating mutation in the gene for *C5* (ref. 12). But given that mating RT2 B6 with A/J mice produced an F1 generation with a very large increase in metastasis (Fig. 1a), we thought that the A/J genome might also contain a metastasis-promoting locus that was either dominant or co-dominant, and this allele turned out to be *Insm1*. Additionally, it has been shown that the *Alk* allele encoded by the B6 genome promotes metastasis more strongly than the *Alk* allele encoded by the C3H inbred line¹³, and we also have evidence that the B6 allele of *Alk* promotes metastasis more strongly than the *Alk* allele of the A/J background (Contractor and Harris, unpublished data). Lastly, we have genetic data that metastasis in RT2 mice is also affected by yet another allelic difference between the A/J and B6 lineages, but have not yet identified the actual gene (Contractor and Harris, unpublished data). Thus four, and possibly more, naturally occurring differences between the A/J and B6 mouse lines have a strong effect on whether the animal has a localized tumor or a metastatic one, an insulinoma or a NF-PanNET. Small-nucleotide polymorphisms that affect tumorigenesis have been identified for many tumor types^{33,34}, but the high number of natural differences between A/J and B6 that affect neuroendocrine tumorigenesis in RT2 mice makes one wonder whether NETs are peculiarly susceptible to naturally occurring genetic diversity.

The subtypes of pancreatic neuroendocrine tumors that can occur in patients show important clinical differences, with nonfunctioning PanNETs being more common and causing worse outcomes than insulinomas¹⁹. Understanding how different tumor subtypes can occur has been an active research area. In animal models for breast and brain tumors, it has been demonstrated that certain

oncogene or tumor suppressor mutations can favor development toward one tumor subtype and not another.^{35,36} In recently published work, mutations in *Men1*, *Daxx*, and *Atrx* were shown to be less common in human insulinomas than in human nonfunctioning tumors, suggesting that subtypes of PanNETs are influenced by the presence of these driver mutations³⁷. But the present work also shows that tumor suppressor gene mutations are not sufficient to explain why different tumor subtypes can occur. Using mice that share a common driver oncogene, we show that tumor subtype is also influenced by naturally occurring genetic diversity, in the form of distinct alleles of the *Insm1* gene. It would be interesting to know whether *Insm1* expression can be directly influenced by mutations in *Men1*, *Daxx*, and *Atrx*, which encode chromatin-remodeling proteins. However, it should also be stated that mouse models do not always reflect how tumors develop in patients; indeed it is not clear whether low *Insm1* expression is a direct cause of nonfunctioning PanNETs in patients, or a byproduct of the cell type from which these tumors originate³⁸.

In patients, a key feature of NF-PanNETs is high rate of metastasis; NF-PanNETs in RT2 AB6F1 mice are likewise highly metastatic. The development of this mouse model may improve the ability to test drugs that could prevent metastasis of PanNETs in vivo. The RT2 mouse has previously been used for in metastasis studies, but comes with important shortcomings: metastasis is less penetrant in RT2 B6 mice, and is complicated by early death due to hypoglycemia. The RT2 AB6F1 mouse overcomes these issues. Metastasis is rapid and highly penetrant especially in male RT2 AB6F1 mice¹², and RT2 AB6F1 mice are not hypoglycemic (Fig. 1d).

Several drugs have shown anti-metastatic activity in mouse models, but there have been no clinical trials designed to test drugs that might slow the risk of metastasis. This is in spite of the fact that metastasis is thought to be the cause of nearly all cancer deaths. There are several pragmatic reasons for the lack of trials on metastasis, including the fact that most clinical trials are performed on late stage, post-metastatic patients in order to overcome the high expense of lengthier trials on earlier stage patients. But another problem may be that spontaneous, synchronized mouse models of metastasis are rare. For this reason, the RT2 AB6F1 mouse model may be of great value. It derives from a mouse in which preclinical successes have led to human clinical trials and to FDA approvals. Although there is not a large population of patients with PanNETs, clinicians who study this disease are highly organized and have shown the ability to perform clinical trials that result in FDA approvals in spite of small patient sets. Patients with PanNETs are often detected before their tumors are metastatic, yet the onset of metastasis is fairly rapid for patients with

nonfunctioning disease. All of these factors—a rapid and validated mouse model, a set of early diagnosed patients, fairly rapid onset of metastasis, and an organized set of clinicians—suggest that the RT2 AB6F1 mouse could prove to be an attractive preclinical model for developing and testing clinically relevant anti-metastatic agents.

Materials and methods

Cell lines

The QGP1 cell line was purchased from the Japan Health Sciences Foundation. The BON1 cell line was a gift from the lab of Kjell Oberg and the CM cell line was a gift from the lab of Paolo Pozzilli. In order to authenticate the cell lines, short tandem repeat analysis was performed by ATCC. The STR results for QGP1 were a 100% match to STR information for QGP1 found in the DSMZ database. The STR results for BON1 were a 100% match to previously published information³⁹. STR results for CM did not match any other cell lines in the databases for ATCC, DSMZ, or EXPASY. STR results for the CM cell line have not previously been published, and are presented in Supplemental Fig. 3. QGP1 and BON1 have previously been tested for mycoplasma but CM cells were not. CM and QGP1 were grown in RPMI media (ThermoFisher) supplemented with 10% fetal bovine serum (Sigma-Aldrich). BON1 cells were grown in Dulbecco's modified Eagle's medium (ThermoFisher) with 10% fetal bovine serum. All lines were grown at 37 °C under 5% CO₂. To decrease heterogeneity, the cell lines were cloned from single colonies before use. CM cells were engineered to express human *Insm1* by using lipofectamine 2000 (ThermoFisher) to transfect a plasmid expressing the human gene under control of the CMV promoter (Origene); *Insm1*-expressing cells were cloned from single transfectants. QGP1 and BON1 were engineered to express luciferase, and then *Insm1* was knocked out by CRISPR, using an EDIT-R lentivirus purchased from Dharmacon (source clone identification number VSGHSM_26789438). Potential low expressers were cloned, and characterized by RTPCR and by western blotting, using an *Insm1* antibody that was a generous gift from Mark Magnuson. Antisera against β -actin (part number A2228) were purchased from Sigma. Genomic DNA from low *Insm1*-expressing clones was subjected to PCR using primers 5'-CAGGTGTTCCCCTGCAAGTA and 5'-CCCAGACAACAGTTCAAGGC; the PCR products were cloned using the TOPO TA system (ThermoFisher), and 12 of the PCR clones were sequenced to confirm the presence of frameshift mutations within the *Insm1* sequence targeted by the EDIT-R lentivirus. BON1 clone 145 showed two new alleles of *Insm1*, each of which had frameshifting deletions: loss of the 10 nt sequence ctcgcccgca, or loss of a single nucleotide, shown emboldened and in lower case within the following

sequence: CCCGGCCcTTACG. QGP1 clone H10 also showed two new alleles of *Insm1*, each of which had frameshifting mutations: loss of two nucleotides, CCCGGCCcTACGCG, or loss of a single nucleotide, CCCGGCCcTTACGCG. A matrigel-coated invasion chamber with 8 μ m pore size (Corning 354480) was used for invasion assays; 20% fetal bovine serum in the upper chamber was used as a chemo-attractant. Three-dimensional growth of cell lines was performed by mixing 1000 cells with 50 μ l of matrigel (Corning 354234), and seeding 5 μ l of this mixture into 96-well plates. After 5 min, 200 μ l of RPMI/10% FBS media were added and the cells were cultured under CO₂ at 37 °C for 2 weeks. *Insm1* siRNAs si-5, si-6, and si-7 were purchased from Dharmacon, and catalog numbers were J-006535-05-002, J-006535-06-002, and J-006535-07-002, respectively

Human and mouse experiments

Human pancreatic neuroendocrine tumors were provided by the Cooperative Human Tissue Network (CHTN), which obtained informed consents from patients. Human experiments were approved by the Institutional Review Board of CHTN. Mouse experiments were approved by the Institutional Animal Care and Use Committee of Rutgers University. RT2 B6 mice were obtained from the National Cancer Institute (Frederick, MD) and bred to C57Bl6/J (Jackson laboratories) for more than 10 generations. A/J mice were purchased from Jackson Laboratories. Mouse husbandry, euthanasia, and autopsy protocols have been previously described¹². *Insm1* genotypes were not assayed until long after the mice had been euthanized and the metastasis and tumor size data were collected. To assay metastasis of the QGP1 cell line, one million cells expressing luciferase were injected into the left ventricles of nude mice, as previously described¹⁴. The day after surgery, and weekly thereafter, mice were sedated with isoflurane, injected with luciferin, and imaged using an IVIS machine. Three weeks after injection, the mice were euthanized by CO₂ asphyxiation and cervical dislocation, and autopsied for metastatic lesions. Organs were examined visually for metastatic lesions. Three organs (liver, pancreas, and both lungs) were also removed, treated with luciferin, and imaged using an IVIS machine. To assay serum insulin and serum glucose, mice were moved to fresh cages with water bottles but no food for 8 h. An ELISA kit for mouse insulin was purchased from RayBiotech and used as recommended by the manufacturer. Serum glucose was measured using a ReliOn Confirm glucose meter and ReliOn Micro Plus test strips

Flow cytometry analysis and cell sorting

Cells were incubated with PE-labeled CD44 antibody (Biolegend) and 7-AAD Viability Dye (Beckman Coulter).

Activity of aldehyde dehydrogenase was determined with AldeFluor Kit (Stem cell Technologies). Flow cytometry analysis and cell sorting were performed using a Cytomics FC500 Flow Cytometer (Beckman Coulter) or a BD Influx High Speed Cell Sorter (BD Biosciences). The purity of sorted cells was >95%.

Genotyping

An SNP assay directed against rs33272877, which differs between the *Insm1* alleles of A/J and C57Bl/6 genomes, was designed and synthesized by ThermoFisher. Outside primer sequences were 5'-CGTGCTGGGCCTGAGT and 5'-GGGCGCCCTTGCT. Reporter sequences were 5'-ACCGCCAGTGCCA and 5'-CCGCCGAGTGCCA. SNP analysis was performed using a Prism 7500 (Applied Biosystems).

Analysis of RNA and protein

Fresh-frozen tumor tissues from male mice were minced in Trizol (ThermoFisher) and homogenized using a Polytron 1200E. Chloroform was then added and the upper aqueous phase was removed after microcentrifugation at 14,000 r.p.m. Ethanol was added and the RNA was then isolated using an RNeasy column (Qiagen) as recommended by the manufacturer. RNA was converted to cDNA using reverse transcription reagents (ThermoFisher). Real-time RT-PCR was then performed, using a Prism 7500 (Applied Biosystems). Most of the RNAs were measured using pre-designed Taqman assays, which were purchased from ThermoFisher. The following assays were designed with Primer3 (<http://bioinfo.ut.ee/primer3/>) and run with SYBR green reagents (ThermoFisher): mouse *Slc24a3* (5'-CCCTCTGGCAAACTGGAAAC and 5'-GGGATCCCTAGTGTGTAGCC); mouse *Cfap61* (5'-AATCACTACCCTCAGCTGCA and 5'-GCCAAAGAAGCATGACCCAT); mouse *Rin2* (5'-AACTCCTGGACCCATCATG and 5'-CATCCGCTGTTGACCTCTTG); mouse *Xrn2* (5'-GAGGTCAAGCTCAGATCCAAA and 5'-GTTCCATGGCAGTAGAGGTTCA); mouse *Crnk1l1* (5' AGAGAAGAAAGGTCCAGGCC and 5'-GCTTGAGGTTAGGCTGGTTG); mouse *Naa20* (5'-AGGGAAGAATGGCATGGACA and 5'-GCTTGTCATGTTGACGGCA); mouse *Nkx2-4* (5'-GCCCCATGAACCTGGAGATT and 5'-CACCTACCACATGCCTCC); human *Rin2* (5'-TCCGCACCATCTCCTGTTTC and 5'-GTCTGGACAAGCGAGGAAGT); mouse *Sox9* (5'-TATCTTCAAGGCGCTGCAAG and 5'-CCCCTCTCGCTTCAGATCAA); mouse *EHF* (5'-GCCCGGCAGAAA GTCTTACT and 5'-TTCCAGTCCGCACACAATGT); mouse *FoxJ1* (5'-CACTCTCATCTGCATGGCCA and 5'-AGGTTGTGGCGGATGGAATT); mouse *Kat14* (5'-ACGAGAGGCTGAAACTGACA and 5'-ACGTCCACTTCCTTCCAGAG); mouse *Zfp120* (5'-AAGCCCAGAAGTTCCGACAT and 5'-AGCAGCGAGATTCCCTGTAGG); mouse *GZF1* (5'-CTCAGCGCAATTCCTGTAC and

5'-GTGAACTGCTTCCCACACTG); and human *GZF1* (5'-TCACTCAGAACCACATGCTG and 5'-AATTCCGCTGGCAAAAGTC).

Analysis of promoter methylation

Tumor DNA was treated using EpiMark Bisulfite Conversion Kit as recommended by the manufacturer (New England Biolabs). Primers were designed using MethPrimer 1.0 (ref. ⁴⁰). Methylation-specific primers were 5'-TTTATTTTACGCGGTTATTTTTC and 5'-ATCGAATCGAAATATTTATCTTCG. Unmethylation-specific primers were 5'-TGTTTGTTTTATTTAATTAGTG and 5'-TCAAATCAAATATTTATCTTCACC.

Immunohistochemistry

For antigen retrieval, slides were boiled for 16 min in 0.93% (v/v) Antigen Unmasking Solution H3301 (Vector Labs), and then slowly cooled to room temperature for 30 min. Primary antibody was guinea pig anti-insulin from Dako (A0564), which was diluted 2000-fold in 10% goat serum/1% BSA. Slides were treated with primary antibody overnight at 4 °C. Secondary antibody was affinity-purified, biotinylated anti-guinea pig IgG from Vector Labs (BA-7000), which was diluted 500-fold in 10% goat serum and 1% BSA. Slides were then treated with Vectastain Elite ABC peroxidase kit (Vector Labs) for 30 min, and with ImmPact DAB peroxidase substrate (Vector Labs SK-4105) for 1min. The slides were counterstained with hematoxylin (Vector Labs).

Statistical analysis

Graphpad Prism 7.04 software was used for statistical analysis. Two-tailed *t*-test was used to compare RNA expression levels from sets of mouse and human tumors. Fisher's exact test was used to compare metastasis frequencies. Pearson correlation analysis was used to compare *Insm1* and *Ins1* expression in human tumors. Nonparametric Mann–Whitney analysis was used to evaluate tumor volumes. Outliers were identified by Rousseeuw analysis ($q = 1\%$).

Acknowledgements

We thank the Raymond and Beverly Sackler Foundation, which funded this study. We also thank Arnie Levine and Robert Harris for very important insights, and Kjell Oberg, Mark Magnuson, and Paolo Pozzilli for contributing reagents. This research was supported by the Rutgers Molecular Imaging Center and by the Flow Cytometry/Cell Sorting shared resource of Rutgers Cancer Institute of New Jersey (P30CA072720).

Author details

¹Institute for Advanced Study, Princeton, NJ, USA. ²Raymond and Beverly Sackler Foundation Laboratory, New Brunswick, NJ, USA. ³Weill Cornell Medicine, New York, NY, USA. ⁴Memorial Sloan Kettering Cancer Center, New York, NY, USA. ⁵Rutgers University Cancer Institute of New Jersey, New Brunswick, NJ, USA. ⁶Department of Pediatrics, Robert Wood Johnson Medical School, New Brunswick, NJ, USA

Conflict of interest

The authors declare that they have no conflict of interest.

Publisher's note

Springer Nature remains neutral with regard to jurisdictional claims in published maps and institutional affiliations.

Supplementary information accompanies this paper at (<https://doi.org/10.1038/s41389-019-0127-1>).

Received: 8 November 2018 Revised: 31 January 2019 Accepted: 8 February 2019

Published online: 22 February 2019

References

- Kuo, E. J. & Salem, R. R. Population-level analysis of pancreatic neuroendocrine tumors 2 cm or less in size. *Ann. Surg. Oncol.* **20**, 2815–2821 (2013).
- Hanahan, D. Heritable formation of pancreatic beta-cell tumours in transgenic mice expressing recombinant insulin/simian virus 40 oncogenes. *Nature* **315**, 115–122 (1985).
- Chiu, C. W., Nozawa, H. & Hanahan, D. Survival benefit with proapoptotic molecular and pathologic responses from dual targeting of mammalian target of rapamycin and epidermal growth factor receptor in a preclinical model of pancreatic neuroendocrine carcinogenesis. *J. Clin. Oncol.* **28**, 4425–4433 (2010).
- Olson, P., Chu, G. C., Perry, S. R., Nolan-Stevaux, O. & Hanahan, D. Imaging guided trials of the angiogenesis inhibitor sunitinib in mouse models predict efficacy in pancreatic neuroendocrine but not ductal carcinoma. *Proc. Natl. Acad. Sci. USA* **108**, E1275–E1284 (2011).
- Yao, J. C. et al. Everolimus for advanced pancreatic neuroendocrine tumors. *N. Engl. J. Med.* **364**, 514–523 (2011).
- Raymond, E. et al. Sunitinib malate for the treatment of pancreatic neuroendocrine tumors. *N. Engl. J. Med.* **364**, 501–513 (2011).
- Reidy-Lagunes, D. L. et al. A phase 2 study of the insulin-like growth factor-1 receptor inhibitor MK-0646 in patients with metastatic, well-differentiated neuroendocrine tumors. *Cancer* **118**, 4795–4800 (2012).
- Ulanet, D. B., Ludwig, D. L., Kahn, C. R. & Hanahan, D. Insulin receptor functionally enhances multistage tumor progression and conveys intrinsic resistance to IGF-1R targeted therapy. *Proc. Natl. Acad. Sci. USA* **107**, 10791–10798 (2010).
- Tang, L. H. et al. Attenuation of the retinoblastoma pathway in pancreatic neuroendocrine tumors due to increased cdk4/cdk6. *Clin. Cancer Res.* **18**, 4612–4620 (2012).
- Sennino, B., Ishiguro-Oonuma, T., Schriver, B. J., Christensen, J. G. & McDonald, D. M. Inhibition of c-Met reduces lymphatic metastasis in RIP-Tag2 transgenic mice. *Cancer Res.* **73**, 3692–3703 (2013).
- Chan, J. A. et al. Phase II trial of cabozantinib in patients with carcinoid and pancreatic neuroendocrine tumors (pNET). *J. Clin. Oncol.* **35**(suppl), 228 (2017).
- Contractor, T. et al. Sexual dimorphism of liver metastasis by murine pancreatic neuroendocrine tumors is affected by expression of complement C5. *Oncotarget* **7**, 30585–30596 (2016).
- Chun, M. G., Mao, J. H., Chiu, C. W., Balmain, A. & Hanahan, D. Polymorphic genetic control of tumor invasion in a mouse model of pancreatic neuroendocrine carcinogenesis. *Proc. Natl. Acad. Sci. USA* **107**, 17268–17273 (2010).
- Choi, S. et al. Bcl-xL promotes metastasis independent of its anti-apoptotic activity. *Nat. Commun.* **7**, 10384 (2016).
- Lopez, T. & Hanahan, D. Elevated levels of IGF-1 receptor convey invasive and metastatic capability in a mouse model of pancreatic islet tumorigenesis. *Cancer Cell* **1**, 339–353 (2002).
- Du, Y. C., Chou, C. K., Klimstra, D. S. & Varmus, H. Receptor for hyaluronan-mediated motility isoform B promotes liver metastasis in a mouse model of multistep tumorigenesis and a tail vein assay for metastasis. *Proc. Natl. Acad. Sci. USA* **108**, 16753–16758 (2011).
- Pyonteck, S. M. et al. Deficiency of the macrophage growth factor CSF-1 disrupts pancreatic neuroendocrine tumor development. *Oncogene* **31**, 1459–1467 (2012).
- Anderson, C. W. & Bennett, J. J. Clinical presentation and diagnosis of pancreatic neuroendocrine tumors. *Surg. Oncol. Clin. N. Am.* **25**, 363–374 (2016).
- Franko, J., Feng, W., Yip, L., Genovese, E. & Moser, A. J. Non-functional neuroendocrine carcinoma of the pancreas: incidence, tumor biology, and outcomes in 2,158 patients. *J. Gastrointest. Surg.* **14**, 541–548 (2010).
- Biondi, C. A. et al. Conditional inactivation of the MEN1 gene leads to pancreatic and pituitary tumorigenesis but does not affect normal development of these tissues. *Mol. Cell Biol.* **24**, 3125–3131 (2004).
- Grant, S. G., Seidman, I., Hanahan, D. & Bautch, V. L. Early invasiveness characterizes metastatic carcinoid tumors in transgenic mice. *Cancer Res.* **51**, 4917–4923 (1991).
- Dorrell, C. et al. The organoid-initiating cells in mouse pancreas and liver are phenotypically and functionally similar. *Stem Cell Res.* **13**, 275–283 (2014).
- Zhang, T., Wang, H., Saunee, N. A., Breslin, M. B. & Lan, M. S. Insulinoma-associated antigen-1 zinc-finger transcription factor promotes pancreatic duct cell trans-differentiation. *Endocrinology* **151**, 2030–2039 (2010).
- Gierl, M. S., Karoulias, N., Wende, H., Strehle, M. & Birchmeier, C. The zinc-finger factor *Insm1* (IA-1) is essential for the development of pancreatic beta cells and intestinal endocrine cells. *Genes Dev.* **20**, 2465–2478 (2006).
- Goto, Y. et al. A novel human insulinoma-associated cDNA, IA-1, encodes a protein with “zinc-finger” DNA-binding motifs. *J. Biol. Chem.* **267**, 15252–15257 (1992).
- Takahashi, K. & Yamanaka, S. Induction of pluripotent stem cells from mouse embryonic and adult fibroblast cultures by defined factors. *Cell* **126**, 663–676 (2006).
- Osipovich, A. B. et al. *Insm1* promotes endocrine cell differentiation by modulating the expression of a network of genes that includes Neurog3 and Ripply3. *Development* **141**, 2939–2949 (2014).
- Kouros-Mehr, H. et al. GATA-3 links tumor differentiation and dissemination in a luminal breast cancer model. *Cancer Cell* **13**, 141–152 (2008).
- Winslow, M. M. et al. Suppression of lung adenocarcinoma progression by Nkx2-1. *Nature* **473**, 101–104 (2011).
- Lawson, D. A. et al. Single-cell analysis reveals a stem-cell program in human metastatic breast cancer cells. *Nature* **526**, 131–135 (2015).
- Mani, S. A. et al. The epithelial-mesenchymal transition generates cells with properties of stem cells. *Cell* **133**, 704–715 (2008).
- Hermann, P. C. et al. Distinct populations of cancer stem cells determine tumor growth and metastatic activity in human pancreatic cancer. *Cell Stem Cell* **1**, 313–323 (2007).
- Deng, N., Zhou, H., Fan, H. & Yuan, Y. Single nucleotide polymorphisms and cancer susceptibility. *Oncotarget* **8**, 110635–110649 (2017).
- Post, S. M. et al. A high-frequency regulatory polymorphism in the p53 pathway accelerates tumor development. *Cancer Cell* **18**, 220–230 (2010).
- Jacques, T. S. et al. Combinations of genetic mutations in the adult neural stem cell compartment determine brain tumour phenotypes. *EMBO J.* **29**, 222–235 (2010).
- Liu, J. C. et al. Combined deletion of Pten and p53 in mammary epithelium accelerates triple-negative breast cancer with dependency on eEF2K. *EMBO Mol. Med.* **6**, 1542–1560 (2014).
- Chan, C. S. et al. ATRX, DAXX or MEN1 mutant pancreatic neuroendocrine tumors are a distinct alpha-cell signature subgroup. *Nat. Commun.* **9**, 4158 (2018).
- Falchetti A. Genetics of multiple endocrine neoplasia type 1 syndrome: what's new and what's old. *F1000Res.* **6**, F1000 Faculty Rev-73. <https://doi.org/10.12688/f1000research.7230.1> (2017).
- Hofving, T. et al. The neuroendocrine phenotype, genomic profile and therapeutic sensitivity of GEPNET cell lines. *Endocr. Relat. Cancer* **25**, 367–380 (2018).
- Li, L. C. & Dahiya, R. MethPrimer: designing primers for methylation PCRs. *Bioinformatics* **18**, 1427–1431 (2002).

ARTICLE

Open Access

Loss of copy of *MIR1-2* increases *CDK4* expression in ileal neuroendocrine tumors

Tanupriya Contractor¹ and Chris R. Harris^{1,2,3}

Abstract

Ileal neuroendocrine tumors (I-NETs) are the most common tumors of the small intestine. Although I-NETs are known for a lack of recurrently mutated genes, a majority of tumors do show loss of one copy of chromosome 18. Among the genes on chromosome 18 is *MIR1-2*, which encodes a microRNA, *MIR1-3p*, with high complementarity to the mRNA of *CDK4*. Here we show that transfection of neuroendocrine cell lines with *MIR1-3p* lowered *CDK4* expression and activity, and arrested growth at the G1 stage of the cell cycle. Loss of copy of *MIR1-2* in ileal neuroendocrine tumors associated with increased expression of *CDK4*. Genetic events that attenuated RB activity, including loss of copy of *MIR1-2* as well as loss of copy of *CDKN1B* and *CDKN2A*, were more frequent in tumors from patients with metastatic I-NETs. These data suggest that inhibitors of *CDK4/CDK6* may benefit patients whose I-NETs show loss of copy of *MIR1-2*, particularly patients with metastatic disease.

Introduction

Neuroendocrine cells are found throughout the body, from the pituitary to the rectum. To prevent hormonal imbalances, these hormone-producing cells are usually under tight growth regulation. But as with many cell types, growth controls can go awry, allowing hyperplasias or even tumors to form. Because neuroendocrine tumors (NETs) often remain well-differentiated and continue to produce hormones, the first symptoms experienced by patients with NETs are often hormone-related. For instance, insulinomas can cause hypoglycemia, while parathyroid tumors can cause frequent kidney stones by altering calcium metabolism.

One of the most common sites of NETs is the ileum of the small intestine^{1–3}. Ileal neuroendocrine tumors (I-NETs) are usually multifocal, well-differentiated tumors that produce the hormone serotonin. Overproduction of serotonin can lead to chronic diarrhea and skin flushing; these symptoms are part of a condition known as carcinoid

syndrome. Carcinoid syndrome is associated with liver metastasis and poor outcome⁴. Notably, the incidence of carcinoid syndrome is increasing⁵. In all, there are about 2500 new cases of I-NETs per year in the United States^{1,2}, making them the most common tumors of the small intestine. A majority of I-NETs are already metastatic by the time of diagnosis. Half of all patients diagnosed with metastatic I-NETs do not survive beyond 5 years¹.

In the clinic, I-NETs are as common as pancreatic neuroendocrine tumors (PNETs)², yet are much less studied. For instance, in Fig. 1, there is a comparison of the number of published abstracts that mention “small intestinal neuroendocrine tumors” with the number of abstracts that mention “pancreatic neuroendocrine tumors.” Part of this research disparity is due to a lack of research tools for I-NETs. I-NET cell lines have been published^{6–8}, but have not been made publicly available. There are also multiple mouse models for PNETs^{9–14}, whereas until very recently¹⁵ I-NETs had not been found in mice. I-NETs also grow slowly, are difficult to detect clinically, and have proven nearly impossible to xenograft into mice.

Another difference that likely fuels the disparity in published work on PNETs and I-NETs is the fact that PNETs

Correspondence: Chris R. Harris (harrisch@cinj.rutgers.edu)

¹Raymond and Beverly Sackler Foundation, New Brunswick, NJ, USA

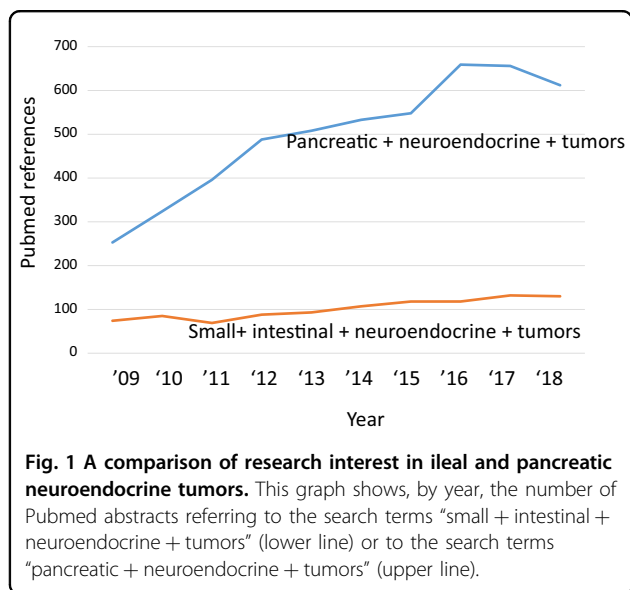
²Department of Surgery, Rutgers Robert Wood Johnson Medical School, New Brunswick, NJ, USA

Full list of author information is available at the end of the article

© The Author(s) 2020



Open Access This article is licensed under a Creative Commons Attribution 4.0 International License, which permits use, sharing, adaptation, distribution and reproduction in any medium or format, as long as you give appropriate credit to the original author(s) and the source, provide a link to the Creative Commons license, and indicate if changes were made. The images or other third party material in this article are included in the article's Creative Commons license, unless indicated otherwise in a credit line to the material. If material is not included in the article's Creative Commons license and your intended use is not permitted by statutory regulation or exceeds the permitted use, you will need to obtain permission directly from the copyright holder. To view a copy of this license, visit <http://creativecommons.org/licenses/by/4.0/>.



have recurrent mutations in genes of great research interest, such as the chromatin remodeling genes *MEN1*, *DAXX*, and *ATRX*¹⁶, whereas the genetic drivers of I-NETs have long remained a mystery¹⁵. I-NETs lack mutations in the genes associated with many cancers, such as *TP53*, *RB1*, *BRCA1*, *MYC*, *AKT1*, or *PIK3CA*. I-NETs are also one of the few types of NETs that are not observed in patients with familial neuroendocrine tumor syndromes, and thus are not caused by alleles of *MEN1* or *MEN2* that produce these syndromes^{17–19}. In certain families, there is evidence for a predisposition to I-NETs, which links to genes other than *MEN1* or *MEN2*^{20–22}. Overall there is a low frequency of mutation in I-NETs, more similar to the low frequency of mutation found in pediatric cancers than to the higher frequency of mutations in most of the tumor types that arise in older patients²³. The only gene recurrently mutated in I-NETs is *CDKN1B*, which is altered in only 5–8% of I-NETs^{23–25}; however, I-NETs have not been reported in mice with *Cdkn1b* mutations.

The only common genetic change in I-NETs is the complete or near-complete loss of one copy of chromosome 18, which is found in well over half of patient samples^{26–28}. While this suggests that chromosome 18 harbors a tumor suppressor gene that prevents I-NETs from forming, no specific gene on chromosome 18 has ever been linked to I-NETs. In this study, we show that a gene on chromosome 18, *MIR1-2*, produces a microRNA that can block expression of *CDK4* and thereby activate the RB1 tumor suppressor protein, resulting in cell cycle arrest of neuroendocrine cell lines. These data suggest that chromosome 18 loss triggers I-NETs by dysregulating the RB pathway and activating the cell cycle. These data suggest that patients with I-NETs may benefit from *CDK4/CDK6* inhibitors.

Results

Because of the high incidence of chromosome 18 loss in I-NETs, we examined this chromosome for the presence of potential tumor suppressor genes. We focused on potential activators of the RB1 tumor suppressor, because the RB1 pathway is associated with several types of NETs^{29–31} and also because this pathway can be attenuated by loss of *CDKN1B*, which is the only gene that is recurrently mutated in I-NETs^{23,25,32}. None of the well-studied activators of RB1, such as the CDK inhibitors *CDKN1A*, *CDKN1B*, *CDKN2A*, and *CDKN2B*, reside on chromosome 18, but we did identify a potential RB1 activator by searching for microRNAs with complementarity to negative regulators of the RB1 pathway. Using TargetScan 7.2 software (http://www.targetscan.org/vert_72/), we searched for broadly conserved miRNAs with 7mer-A1, 7mer-M8, or 8mer complementarity³³ to the mRNAs of *CDK4*, *CDK6*, *CCND1*, *CCND2*, and *CCND3*. We then used the UCSC Genome Browser (<http://genome.ucsc.edu/>) to match these microRNAs to the chromosomes of the genes encoding them within human genome release GRCh38. Out of 105 microRNA genes identified by this approach, only one, *MIR1-2*, resided on chromosome 18 (Supplementary Table 1). *MIR1-2* encodes MIR1-3p, which is complementary to sequences within the untranslated regions (UTRs) of mRNAs for *CDK4*, *CDK6*, *CCND1*, and *CCND2*. Interestingly, decreased MIR1-3p expression has previously been detected in patients with advanced I-NETs^{34,35}.

Neuroendocrine tumor cell lines were transfected with MIR1-3p. Because there are no publicly available cell lines derived from serotonin-producing ileal NETs, we performed these experiments in BON1 and QGP1, two pancreatic NET cell lines that were derived from serotonin-producing tumors^{36,37}. At the mRNA level, there was no statistically significant decrease in the expression of *CDK6* or *CCND1* following MIR1-3p transfection (Fig. 2a), and *CCND2* was not assayable due to poor expression in both cell lines. However, expression of *CDK4* by both BON1 and QGP1 decreased following transfection with MIR1-3p (Fig. 2a). Transfection of MIR1-3p also decreased the amount of CDK4 protein produced by the two cell lines, as shown by Western blot (Fig. 2b). Activated CDK4 causes phosphorylation of RB1 at amino acids 807 and 811, and the amount of RB1 phosphorylated on these residues decreased in cells treated with MIR1-3p (Fig. 2b). Thus MIR1-3p decreases the activity of CDK4, which should increase the activity of RB. Transfection of MIR1-3p also decreased the rate of growth of both BON1 and QGP1 (Fig. 2c, d; see also Videos 1–4 in Supplementary material).

Since activated RB1 arrests growth at the G1 phase of the cell cycle³⁸, we next performed cell cycle analysis on the MIR1-3p-treated cells. For this analysis, the BON1

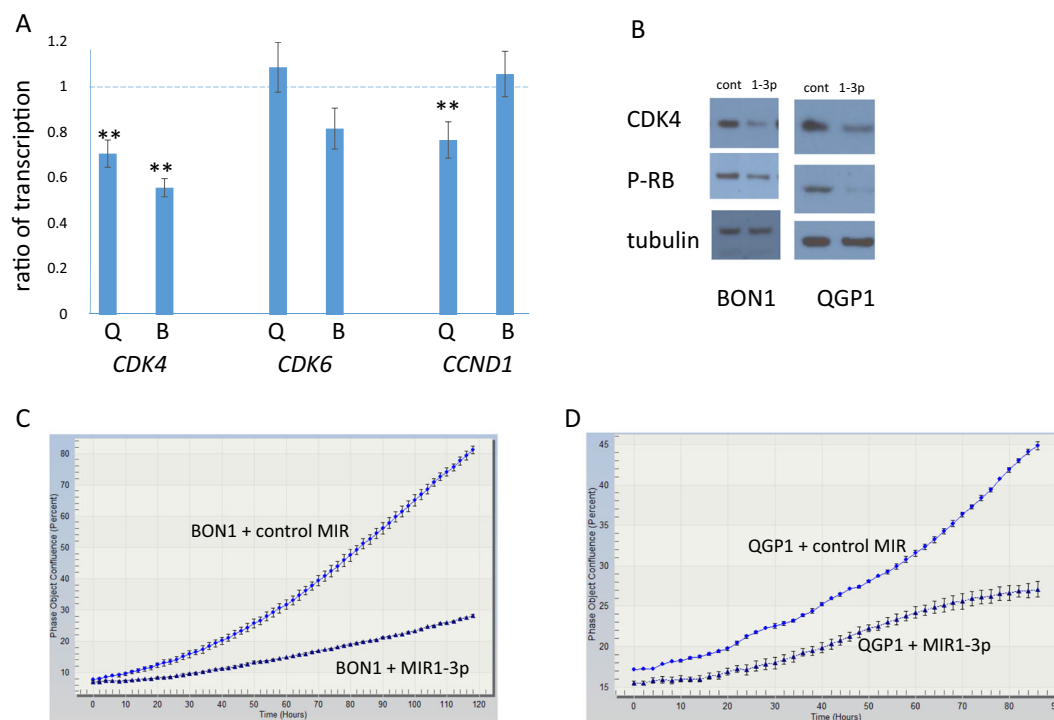


Fig. 2 Effect of MIR1-3p on expression of RB pathway genes in neuroendocrine tumor cell lines. **a** Ratio of transcription refers to mRNA expression following transfection with microRNA MIR1-3p, divided by mRNA expression following transfection with a control microRNA. Values below 1 indicate repression by MIR1-3p. The assayed mRNAs were *CDK4*, *CDK6*, and *CCND1*, which were normalized to expression of *RPLPO*. Statistically significant expression differences of *CDK4* ($p < 0.05$) between cells transfected with MIR1-3p and control microRNA were determined by two-tailed *T*-test and are indicated by asterisks. Expression effects were evaluated in two neuroendocrine cell lines, QGP1 (denoted as Q) and BON1 (denoted as B). **b** QGP1 and BON1 were transfected with control microRNA or with MIR1-3p. After 48 h, protein was collected and separated by SDS-polyacrylamide gel electrophoresis. The results of Western blotting with antisera against CDK4, Phospho-RB1(807/811) and β -tubulin are shown. **c** and **d** The BON1 **c** and QGP1 **d** cell lines were transfected with MIR1-3p or with a control microRNA, and then growth was measured every 2 h using an Incucyte ZOOM live cell microscope. Quantification of plate confluence was performed using ZOOM 2016B software.

and QGP1 cell lines were transfected with MIR1-3p or with control microRNA for 24 h, and then treated with nocodazole for another 16 h²⁹. Nocodazole caused a G2 cell cycle arrest, as shown in the cells treated with control microRNA (Fig. 3a, b). But cells pre-treated with MIR1-3p were enriched in G1-phase cells, as would be expected for cells in which RB1 has been activated. Together these data indicate that MIR1-3p expression has a negative effect on growth of neuroendocrine cell lines, by decreasing the expression of CDK4.

MIR1-3p is complementary to a short segment within the 3' UTR of *CDK4* mRNA. Fusing the *CDK4* UTR to a gene encoding firefly luciferase enabled MIR1-3p to negatively regulate luciferase expression (Fig. 3c). Conversely, following site-directed mutagenesis to remove the complementary sequence from the UTR, MIR1-3p was no longer able to regulate expression of the luciferase/*CDK4* fusion gene (Fig. 3c).

A set of 57 flash-frozen human I-NETs was purchased from the Cooperative Human Tissue Network (CHTN). Patients ranged in age from 41 to 89, but 95% of the

patients were 49 or older. The average age of these patients was 61. Both sexes were represented (51% male), but the samples were not racially diverse (93% Caucasian). There was no clinical data available for these patients other than the fact that 51% of patients had localized disease, and 49% of the patients had distal metastases. Distal metastases usually localized to the liver, but one patient had a metastatic neuroendocrine lesion on an ovary. Genomic DNA was prepared from these tumor samples in order to determine the copy number of the *MIR1-2* gene for each patient.

Expression of *CDK4* mRNA increased in tumors with loss of copy of *MIR1-2* (Fig. 4a). Conversely, expression of MIR1-3p tended to decrease in tumors with loss of copy of *MIR1-2*, although this result was not statistically significant (Fig. 4b). Plotting expression of MIR1-3p and *CDK4* mRNA revealed that these two RNAs were negatively correlated (Fig. 4c). Combined with the results from the cell line experiments, these data suggest that loss of chromosome 18 may lower expression of MIR1-3p, which can increase expression of CDK4 and

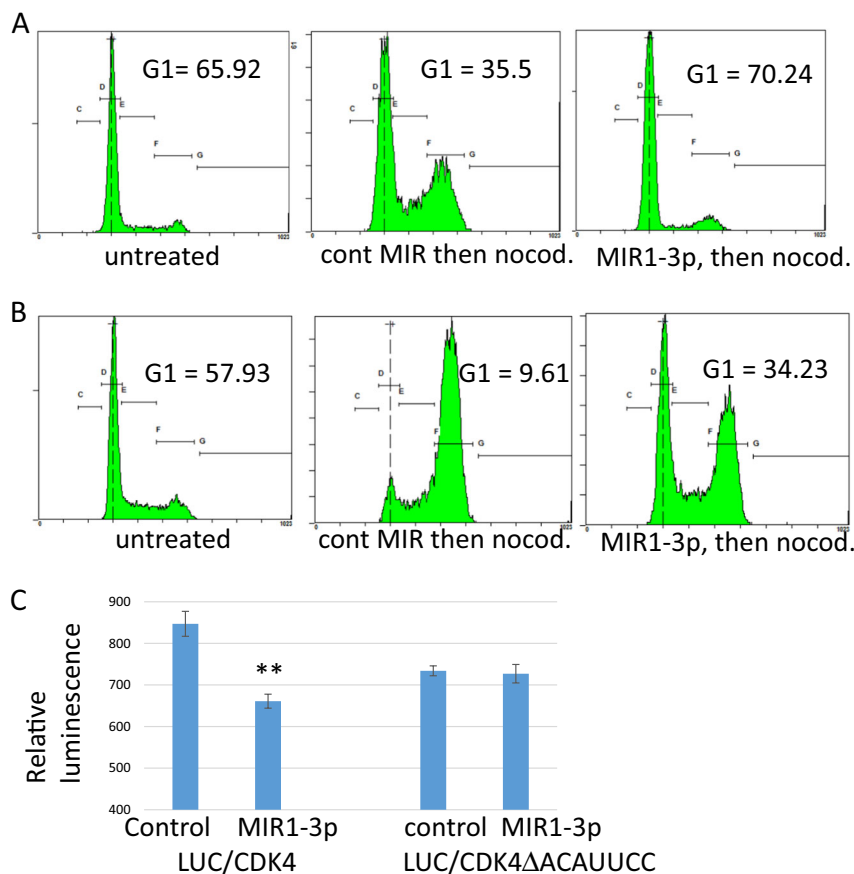


Fig. 3 Effects of MIR1-3p on the cell cycle in neuroendocrine tumor cell lines. **a** and **b** The QGP1 **a** and BON1 **b** cell lines were transfected with MIR1-3p or with a control microRNA. 1 day later, the cells were treated with nocodazole for 16 h, followed by propidium iodide treatment and flow cytometry to determine effects on cell cycle. Untreated cells are shown in the first panel, control microRNA/nocodazole-treated cells are shown in the second panel, and MIR1-3p/nocodazole-treated cells are shown in the third panel. The percentage of cells in G1 are indicated for each treatment. **c** The cell line H1299 was transfected with control microRNA or with MIR1-3p, along with plasmids encoding either LUC/CDK4, which encodes a luciferase gene fused to the 3' UTR of *CDK4*, or to LUC/CDK4ΔACAUUCC, which is nearly the same fusion gene except that it lacks the 7-mer sequence that is complementary to MIR1-3p. Statistical significance between control-treated and MIR1-3p-treated cells was determined by two-tailed *T*-test.

cause dysregulated growth of enteroendocrine cells of the ileum.

We also assayed the tumor DNAs for mutations and copy number alterations in other genes of the RB pathway. Loss of copy of the *MIR1-2* gene was by far the most common event, occurring in 63% of tumors (Fig. 5a). *CDKN1B* mutations, and loss of copy of *CDKN1B* were uncommon. The frequencies of these alterations in *CDKN1B* within this data set were consistent with previous reports^{23,25}. Loss of copy of another CDK inhibitor, *CDKN2A*, was as common as alterations in *CDKN1B* (Fig. 5a). Although amplifications of the *CDK4* and *CDK6* genes have been detected in pancreatic NETs²⁹, these genes were not amplified in any of the 57 I-NET samples (Fig. 5a). There were rare amplifications of the D-cyclin genes (*CCND1*, *CCND2*, and *CCND3*); interestingly, each of these events occurred in tumors from patients with metastatic disease.

Attenuation of the RB pathway has been linked to metastasis of other tumor types^{39–41}, and appears to be the case for I-NETs as well. As shown in Fig. 5b, tumors that showed copy number or sequence alterations of one or more RB pathway genes were more likely to derive from patients with metastatic disease. *MIR1-2* loss alone also correlated with metastasis, as 82% of I-NETs from patients with distal metastasis had a loss of copy of *MIR1-2*, but *MIR1-2* was lost in only 45% of patients with localized disease (Fig. 5c).

Discussion

There is a clinical need for better treatments of metastatic I-NETs. Primary I-NETs remain difficult to detect, and at initial diagnosis most patients already have metastatic disease. Indeed I-NETs are one of the few tumor types for which there has been a recent increase in the

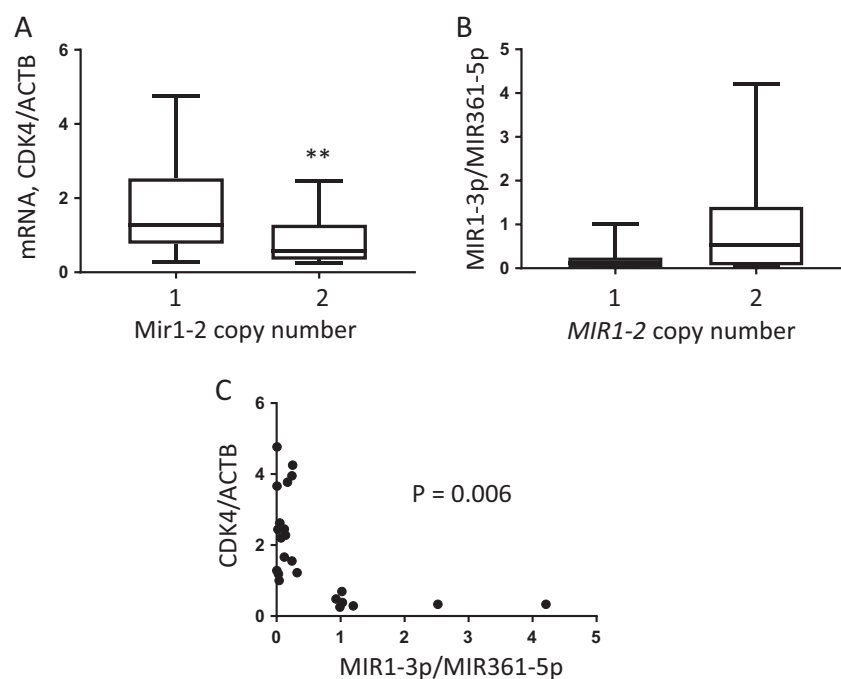


Fig. 4 Expression of *MIR1-3p* and *CDK4* in human ileal neuroendocrine tumors with different copy numbers of *MIR1-2*. **a** Comparison of expression of *CDK4* mRNA by human I-NETs with loss of copy of *MIR1-2* (denoted as 1) to expression of *CDK4* by tumors with a normal copy number of *MIR1-2* (denoted as 2). *CDK4* mRNA was assayed by real-time RT-PCR and normalized to expression of a housekeeper, *ACTB*. Statistical significance was determined by Mann–Whitney analysis ($p < 0.05$). **b** Comparison of expression of *MIR1-3p* by human I-NETs with loss of copy of *MIR1-2* (denoted as 1) to expression by tumors with a normal copy number of *MIR1-2* (denoted as 2). *MIR1-3p* expression was assayed by real-time RT-PCR and normalized to expression of a housekeeper, *MIR361-5p*. Although there is a trend toward lower expression in tumors with loss of copy, this difference was not statistically significant by Mann–Whitney analysis ($p = 0.12$). **c** Expression of *MIR1-3p* and *CDK4* by individual I-NETs is plotted. The Spearman correlation coefficient was $r = -0.556$, and there was a statistically significant correlation with a p value of 0.006.

percentage of advanced disease among newly diagnosed patients⁵. Surgical resection is the most effective treatment for I-NETs, but resection is not always possible for patients with a high metastatic burden. Pharmacologically, I-NETs do not respond to chemotherapy and are not thought to be good candidates for new immunotherapies due to a low number of tumor-specific antigens. Personalized medicine approaches for I-NETs are limited by the low number of mutations. Patients can respond to mTOR inhibitors⁴², and to somatostatin analogs such as octreotide⁴³. There have been promising results from recent clinical trials in which patients with highly metastatic I-NETs were treated with toxic, radiolabeled compounds that are attached to somatostatin analogs^{44,45}.

CDK4/CDK6 inhibitors are among the most exciting new anti-cancer drugs of the past 10 years, and are approved by the FDA for patients with ER+HR– breast cancer⁴⁶. Our previous report on the incidence of CDK4 overexpression/gene amplification in pancreatic NETs, combined with the response of PNET cell lines to CDK4/CDK6 inhibitors particularly in combination with mTOR inhibitors²⁹, helped lead to multiple ongoing clinical trials

for neuroendocrine and breast tumors (ClinicalTrials.gov Identifiers NCT02420691, NCT03070301, and NCT02732119). But patients with I-NETs were excluded from these trials due to a lack of data about whether CDK4 is important in the biology of I-NETs. The present report strongly suggests that patients with I-NETs could benefit from treatment with CDK4/CDK6 inhibitors.

We demonstrate that *MIR1-2* encodes a microRNA that negatively regulates expression of *Cdk4*. *MIR1-2* resides on chromosome 18, whose loss is the most frequent genetic event in I-NETs, suggesting that *MIR1-2* loss is a genetic driver of these tumors. Transfection of neuroendocrine tumor cell lines with the product of *MIR1-2*, *MIR1-3p*, decreased expression of *CDK4*, decreased phosphorylation of RB, prevented cell growth and caused cell cycle arrest. In patient samples, the copy number of *MIR1-2* negatively associated with *MIR1-3p* expression and positively associated with *CDK4* expression. Loss of copy of *MIR1-2* was particularly common in patients with advanced I-NETs. In agreement with these data, two recent studies linked a number of microRNAs with I-NET biology, including *MIR1-3p*, which was found in lowered abundance in patients with advanced I-NETs^{34,35}.

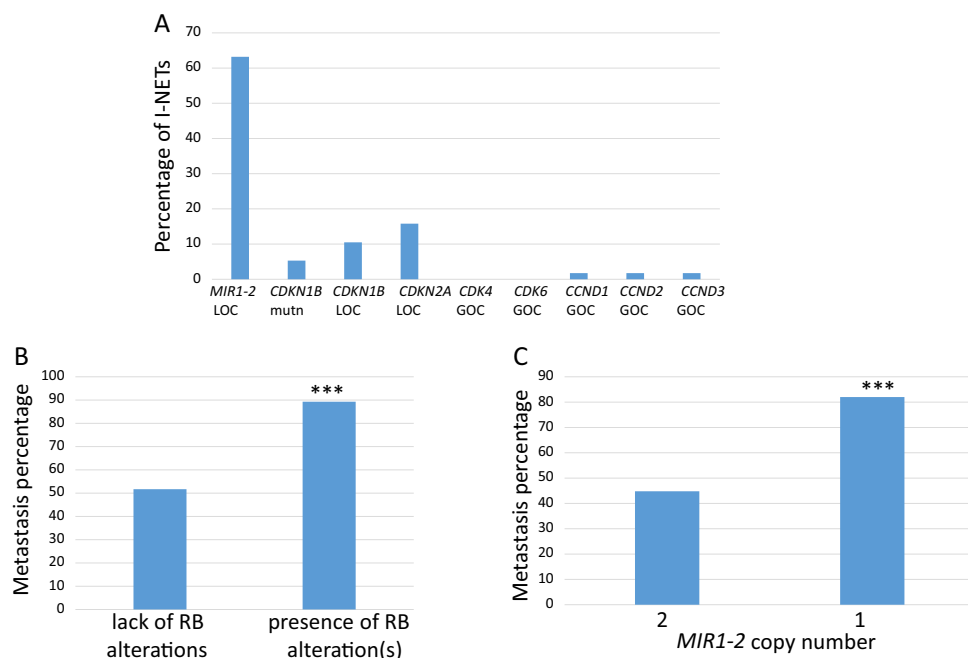


Fig. 5 Copy numbers of *MIR1-2* and other *RB* pathway genes in metastatic or localized human ileal neuroendocrine tumors. **a** A total of 57 I-NETs were analyzed for loss of copy (LOC) of *RB* activators *MIR1-2*, *CDKN1B*, and *CDKN2A*, for mutations in *CDKN1B*, or for gain of copy (GOC) of *RB* suppressors *CDK4*, *CDK6*, *CCND1*, *CCND2*, and *CCND3*. The percentage of tumors showing each of these genetic events is indicated. **b** This figure shows the incidence of metastatic disease among patients whose tumors lacked any of the genetic changes in the *RB* pathway shown in **a**, compared to the incidence of metastatic disease among patients whose tumors had at least one of the genetic changes in **a**. Statistical significance was determined by Fisher's exact test ($p < 0.01$). **c** This figure shows the incidence of metastatic disease among patients whose tumors had two copies of the *MIR1-2* gene (2) compared to the incidence of metastatic disease among patients whose tumors had loss of copy of *MIR1-2* (1). Statistical significance was determined by Fisher's exact test ($p < 0.01$).

Although I-NETs are usually already metastatic at diagnosis, several of the patients in the data base had no distal metastasis, but still showed loss of copy of *MIR1-2*. These patients may be at greater risk for later development of distal metastasis.

Because of the slow growth rate of I-NETs, clinical trials can be long and costly; trials designed to test the efficacy of drugs that block cell cycle, like CDK4/6 inhibitors, also take longer than trials on drugs that cause cell apoptosis. Interestingly, in a recent study, a CDK4/6 inhibitor was tested in a set of 15 patients with various tumor types. Two of the patients showed an objective response, and one of the responding patients had an I-NET⁴⁷. To our knowledge, this is the only literature record in which a patient with an I-NET was treated with a CDK4/6 inhibitor, and it is particularly interesting that a drug designed to prevent cell growth actually caused this I-NET to shrink. A recent report does suggest that CDK4/6 inhibitors can cause tumors to shrink by activating natural killer cells, allowing the immune system to attack tumors⁴⁸. If CDK4/6 inhibitors can cause an objective response in a significant number of I-NETs, then perhaps shorter and less costly trials on these tumors can be designed. These trials may also have a better chance of

success by stipulating that patients' tumors show loss of copy of *MIR1-2*. In the future a personalized medicine approach, using copy number of *MIR1-2* to determine which patients should be treated with CDK4/6 inhibitors, may allow these drugs to reduce the chances of progression by some early stage patients, while also increasing the chances of objective responses of late stage patients.

The *RB* pathway is attenuated in many types of NETs. For instance, in previous work we showed overexpression of CDK4 in 75% of pancreatic NETs, as well as common copy number amplifications of the *CDK4* and *CDK6* genes²⁹. Another type of neuroendocrine tumor, small cell lung tumors, nearly always contains *RB1* mutations³⁰. *Rb1*+/- mice were initially developed to model retinoblastoma, but instead of retinoblastomas these mice developed a large variety of NETs^{31,49}. RT2 mice, in which *RB* is inactivated by expression of SV40 T-antigen, can also develop several types of NETs (insulinomas, non-functioning pancreatic NETs, or duodenal NETs), depending on genetic background^{9,10,50–52}. Importantly, we recently found two genetic backgrounds in which RT2 mice can also produce I-NETs¹⁵. For I-NETs to appear in these backgrounds, the expression of SV40 T-antigen was required, as was elevated activity of IGF2. The presence of

I-NETs in these RB-inactivated mice provides further support for the importance of RB pathway attenuation in ileal neuroendocrine tumorigenesis.

Materials and methods

Analysis of gene expression in human I-NETs

Flash-frozen human I-NETs were obtained from the CHTN. Informed consent was obtained from CHTN and experiments were approved by the Institutional Review Boards of CHTN. Genomic DNA was prepared from 57 tumors using a Wizard kit from Promega. RNA was isolated from 42 tumors using an RNeasy kit from Qiagen. RNA was converted into cDNA using a reverse transcription reagents kit (ThermoFisher), and *CDK4* was quantitated using real-time RT-PCR, then normalized to the expression of β -actin. MicroRNA was prepared from 23 frozen tumors using a miRNeasy kit from Qiagen and converted into cDNA using Taqman advanced miRNA cDNA kit (ThermoFisher). MIR1-3p expression was quantitated using real-time RT-PCR, and normalized to expression of MIR361-5p, which was recommended as a housekeeping microRNA by ThermoFisher. All Taqman assays were purchased from ThermoFisher.

Copy number analysis

Copy number within tumor DNA was determined by real-time RT-PCR, using an Applied Biosystems Prism 7500 and CopyCaller software, as recommended by the manufacturer. Copy number assays were purchased from ThermoFisher and were as follows: *MIR1-2* (Hs06506989_cn); *CCND1* (Hs00377865_cn); *CCND2* (Hs00394283_cn); *CCND3* (Hs02982157_cn); *CDKN1B* (Hs02136152_cn); *CDKN2A* (Hs03714372_cn); *CDK4* (Hs01071103_cn); and *CDK6* (Hs00389416_cn). Copy numbers of *RNASEP* and *TERT* were used for normalization of input DNA.

Analysis of *CDKN1B* sequence

For sequencing of *CDKN1B*, the two coding exons of *CDKN1B* were amplified from tumor DNA by PCR. PCR primers were 5'-TATCGTGAGGTCTGAAGGCC and 5'-GTTTATCAACGGTCCGCCTC (exon 2) and 5' GCGCT TTGTTTTGTTTCGGTT and 5' AATACGCCGAAAAG CAAGCT (Exon 1). The exon 2 sequencing primer was 5' GGAGGTAGTGGGTTTTTCA and the exon 1 sequencing primer was 5'GCAAGCTAAGGTAAACAC. Sanger sequencing was performed by GeneWiz.

Analysis of the effects of MIR1-3p expression in human neuroendocrine tumor cell lines

The QGP1 cell line was purchased from the Japan Health Sciences Foundation and was grown under 5% CO₂ at 37 °C in RPMI media supplemented with 10% fetal bovine serum (Sigma-Aldrich). The BON1 cell line was a

gift from the lab of Kjell Oberg and was grown under 5% CO₂ at 37 °C in DMEM media supplemented with 10% fetal bovine serum. The QGP1 and BON1 cell lines were authenticated as previously described¹⁰. MIR1-3p (MC10617) was purchased from ThermoFisher, along with a negative control (4464058). MicroRNAs were transfected using RNAiMax (ThermoFisher) as described by the manufacturer. Experiments were performed in triplicate. A total of 200,000 cells were reverse transfected with 20 pmol of microRNA in the presence of 4 μ l of RNAiMAX. After 48 h, transfected cells were harvested for RNA or protein. For measurement of cell growth effects, microRNA was reverse transfected into cells, then 16 h later the wells were analyzed every 2 h using an Incucyte ZOOM live cell microscope (Essen Bioscience). Cell confluence and statistical differences were determined using ZOOM 2016B software. For measurement of cell cycle effects, microRNA was transfected for 24 h, after which cells were treated for 16 h with 100 ng/ml nocodazole (Sigma-Aldrich). Cells were harvested by trypsinization 16 h after nocodazole treatment, washed in PBS, and fixed in 70% ethanol. Propidium iodide was added for cell-cycle analysis, which was performed on a Cytomics FC500 Flow Cytometer (Beckman Coulter). Antisera against CDK4 and β -tubulin were purchased from Novus (NBP1-31308 and NB600-936, respectively). Antisera against Phospho-RB (Ser807/811) were purchased from Cell Signaling (8516S).

Analysis of expression effects caused by MIR1-3p and the UTR of *CDK4*

To assay the effect of the 3' UTR of human *CDK4* mRNA on expression of firefly luciferase, the UTR was amplified from normal human genomic DNA by PCR, using primers 5'-CGCCGTGTAATTCTAGAAAGCT GCCATTTCCCTTCTG-3' and 5'-GCCGCCCGACTC TAGACACGCCCGCCTAAAATC-3'. The PCR product was inserted into XbaI-digested pGL3-control vector (Promega) using an InFusion kit (Takeda). Site-directed mutagenesis using a Q5 kit (New England Biolabs) was performed to remove the luciferase/*CDK4* sequence that was complementary to MIR1-3p. Site-directed mutagenesis utilized primers 5'-CCTCCACCTCTCCTTTT-3' and 5'-CATTAAGGCAGCAAAGTAATC-3'. The H1299 large cell (neuroendocrine) lung cell line was a gift from the laboratory of Arnold Levine, and was plated in 12-well dishes at a concentration of 100,000 cells/well. 0.5 μ g of firefly-reporter plasmid was transfected along with 20 pmol of microRNA and 2 ng of renilla-reporter plasmid pRL-TK (Promega). 1.25 μ l of lipofectamine 2000 (ThermoFisher) was used as a transfection reagent. Transfections were performed in triplicate for 56 h, after which the activities of firefly and Renilla luciferases were determined.

Statistical analysis

Graphpad Prism 7.04 software was used for statistical analysis. Comparisons of cell line expression of mRNAs and luciferase were performed by two-tailed *T*-test. Tumor expression of MIR1-3p and *CDK4* were not a Gaussian distribution, and were analyzed by non-parametric Mann–Whitney test. Outliers were identified by Rout analysis. Correlation between expression of MIR1-3 and *CDK4* was evaluated by Pearson test. Comparison of metastasis percentages by tumors lacking or containing copy number changes in *MIR1-2* or in a larger set of *RBI* pathway genes was performed by two-sided Fisher's exact test.

Acknowledgements

This work was funded by the Raymond and Beverly Sackler Foundation. We sincerely thank Darren Carpizo, Arnold Levine, and Evan Vosburgh for contributing reagents and for helpful comments on this manuscript. We also thank Xin Yu, Wen Xie, and the Rutgers Advanced Microscopy Shared Resource for help with cell growth experiments.

Author details

¹Raymond and Beverly Sackler Foundation, New Brunswick, NJ, USA.

²Department of Surgery, Rutgers Robert Wood Johnson Medical School, New Brunswick, NJ, USA. ³Rutgers Cancer Institute of New Jersey, New Brunswick, NJ, USA

Conflict of interest

The authors declare that they have no conflict of interest.

Publisher's note

Springer Nature remains neutral with regard to jurisdictional claims in published maps and institutional affiliations.

Supplementary Information accompanies this paper at (<https://doi.org/10.1038/s41389-020-0221-4>).

Received: 19 August 2019 Revised: 24 February 2020 Accepted: 25 February 2020

Published online: 20 March 2020

References

1. Yao, J. C. et al. One hundred years after "carcinoid": epidemiology of and prognostic factors for neuroendocrine tumors in 35,825 cases in the United States. *J. Clin. Oncol.* **26**, 3063–3072 (2008).
2. Dasari, A. et al. Trends in the incidence, prevalence, and survival outcomes in patients with neuroendocrine tumors in the United States. *JAMA Oncol.* **3**, 1335–1342 (2017).
3. Modlin, I. M., Champaneria, M. C., Chan, A. K. & Kidd, M. A three-decade analysis of 3,911 small intestinal neuroendocrine tumors: the rapid pace of no progress. *Am. J. Gastroenterol.* **102**, 1464–1473 (2007).
4. Boudreaux, J. P. et al. The NANETS consensus guideline for the diagnosis and management of neuroendocrine tumors: well-differentiated neuroendocrine tumors of the jejunum, ileum, appendix, and cecum. *Pancreas* **39**, 753–766 (2010).
5. Halperin, D. M. et al. Frequency of carcinoid syndrome at neuroendocrine tumour diagnosis: a population-based study. *Lancet Oncol.* **18**, 525–534 (2017).
6. Kolby, L. et al. A transplantable human carcinoid as model for somatostatin receptor-mediated and amine transporter-mediated radionuclide uptake. *Am. J. Pathol.* **158**, 745–755 (2001).
7. Pfragner, R. et al. Establishment and characterization of three novel cell lines—P-ST5, L-ST5, H-ST5-derived from a human metastatic midgut carcinoid. *Anticancer Res.* **29**, 1951–1961 (2009).
8. Pfragner, R. et al. Establishment of a continuous cell line from a human carcinoid of the small intestine (KRJ-I). *Int. J. Oncol.* **8**, 513–520 (1996).
9. Hanahan, D. Heritable formation of pancreatic beta-cell tumours in transgenic mice expressing recombinant insulin/simian virus 40 oncogenes. *Nature* **315**, 115–122 (1985).
10. Kobayashi, S. et al. Alleles of *Insm1* determine whether RIP1-Tag2 mice produce insulinomas or nonfunctioning pancreatic neuroendocrine tumors. *Oncogenesis* **8**, 16 (2019).
11. Shen, H. C. et al. Recapitulation of pancreatic neuroendocrine tumors in human multiple endocrine neoplasia type I syndrome via *Pdx1*-directed inactivation of *Men1*. *Cancer Res.* **69**, 1858–1866 (2009).
12. Crabtree, J. S. et al. A mouse model of multiple endocrine neoplasia, type 1, develops multiple endocrine tumors. *Proc. Natl Acad. Sci. USA* **98**, 1118–1123 (2001).
13. Wong, C. et al. Two well-differentiated pancreatic neuroendocrine tumor mouse models. *Cell Death Differ.* **27**, 269–283 (2019).
14. Du, Y. C., Lewis, B. C., Hanahan, D. & Varmus, H. Assessing tumor progression factors by somatic gene transfer into a mouse model: *Bcl-xL* promotes islet tumor cell invasion. *PLoS Biol.* **5**, e276 (2007).
15. Contractor, T. et al. *IGF2* drives formation of ileal neuroendocrine tumors in patients and mice. *Endocr. Relat. Cancer* **27**, 175–186 (2020).
16. Jiao, Y. et al. *DAXX/ATRX*, *MEN1*, and *mTOR* pathway genes are frequently altered in pancreatic neuroendocrine tumors. *Science* **331**, 1199–1203 (2011).
17. Chandrasekharappa, S. C. et al. Positional cloning of the gene for multiple endocrine neoplasia-type 1. *Science* **276**, 404–407 (1997).
18. Donis-Keller, H. et al. Mutations in the *RET* proto-oncogene are associated with *MEN 2A* and *FMTC*. *Hum. Mol. Genet.* **2**, 851–856 (1993).
19. Mulligan, L. M. et al. Germ-line mutations of the *RET* proto-oncogene in multiple endocrine neoplasia type 2A. *Nature* **363**, 458–460 (1993).
20. Dumanski, J. P. et al. A *MUTYH* germline mutation is associated with small intestinal neuroendocrine tumors. *Endocr. Relat. Cancer* **24**, 427–443 (2017).
21. Neklason, D. W., VanDerslice, J., Curtin, K. & Cannon-Albright, L. A. Evidence for a heritable contribution to neuroendocrine tumors of the small intestine. *Endocr. Relat. Cancer* **23**, 93–100 (2016).
22. Sei, Y. et al. A hereditary form of small intestinal carcinoid associated with a germline mutation in inositol polyphosphate multikinase. *Gastroenterology* **149**, 67–78 (2015).
23. Francis, J. M. et al. Somatic mutation of *CDKN1B* in small intestine neuroendocrine tumors. *Nat. Genet.* **45**, 1483–1486 (2013).
24. Banck, M. S. et al. The genomic landscape of small intestine neuroendocrine tumors. *J. Clin. Invest.* **123**, 2502–2508 (2013).
25. Maxwell, J. E. et al. Somatic alterations of *CDKN1B* are associated with small bowel neuroendocrine tumors. *Cancer Genet.* **208**, 564–570 (2015).
26. Wang, G. G. et al. Comparison of genetic alterations in neuroendocrine tumors: frequent loss of chromosome 18 in ileal carcinoid tumors. *Mod. Pathol.* **18**, 1079–1087 (2005).
27. Zhao, J. et al. Genomic alterations in well-differentiated gastrointestinal and bronchial neuroendocrine tumors (carcinoids): marked differences indicating diversity in molecular pathogenesis. *Am. J. Pathol.* **157**, 1431–1438 (2000).
28. Lollgen, R. M., Hessman, O., Szabo, E., Westin, G. & Akerstrom, G. Chromosome 18 deletions are common events in classical midgut carcinoid tumors. *Int. J. Cancer* **92**, 812–815 (2001).
29. Tang, L. H. et al. Attenuation of the retinoblastoma pathway in pancreatic neuroendocrine tumors due to increased *cdk4/cdk6*. *Clin. Cancer Res.* **18**, 4612–4620 (2012).
30. van Meerbeeck, J. P., Fennell, D. A. & De Ruysscher, D. K. Small-cell lung cancer. *Lancet* **378**, 1741–1755 (2011).
31. Matoso, A., Zhou, Z., Hayama, R., Flesken-Nikitin, A. & Nikitin, A. Y. Cell lineage-specific interactions between *Men1* and *Rb* in neuroendocrine neoplasia. *Carcinogenesis* **29**, 620–628 (2008).
32. Banck, M. S. & Beutler, A. S. Advances in small bowel neuroendocrine neoplasia. *Curr. Opin. Gastroenterol.* **30**, 163–167 (2014).
33. Agarwal, V., Bell, G. W., Nam, J. W. & Bartel, D. P. Predicting effective microRNA target sites in mammalian mRNAs. *Elife* **4**, e05005 (2015).
34. Avidsson, Y. et al. miRNA profiling of small intestinal neuroendocrine tumors defines novel molecular subtypes and identifies miR-375 as a biomarker of patient survival. *Mod. Pathol.* **31**, 1302–1317 (2018).
35. Miller, H. C. et al. MicroRNAs associated with small bowel neuroendocrine tumours and their metastases. *Endocr. Relat. Cancer* **23**, 711–726 (2016).
36. Evers, B. M., Ishizuka, J., Townsend, C. M. Jr. & Thompson, J. C. The human carcinoid cell line, BON. A model system for the study of carcinoid tumors. *Ann. N. Y. Acad. Sci.* **733**, 393–406 (1994).

37. Doihara, H. et al. QGP-1 cells release 5-HT via TRPA1 activation; a model of human enterochromaffin cells. *Mol. Cell. Biochem.* **331**, 239–245 (2009).
38. Weinberg, R. A. The retinoblastoma protein and cell cycle control. *Cell* **81**, 323–330 (1995).
39. Kumar, A. et al. Substantial interindividual and limited intraindividual genomic diversity among tumors from men with metastatic prostate cancer. *Nat. Med.* **22**, 369–378 (2016).
40. Robinson, D. et al. Integrative clinical genomics of advanced prostate cancer. *Cell* **162**, 454 (2015).
41. Thangavel, C. et al. RB loss promotes prostate cancer metastasis. *Cancer Res.* **77**, 982–995 (2017).
42. Yao, J. C. et al. Everolimus for the treatment of advanced, non-functional neuroendocrine tumours of the lung or gastrointestinal tract (RADIANT-4): a randomised, placebo-controlled, phase 3 study. *Lancet* **387**, 968–977 (2016).
43. Rinke, A. et al. Placebo-controlled, double-blind, prospective, randomized study on the effect of octreotide LAR in the control of tumor growth in patients with metastatic neuroendocrine midgut tumors: a report from the PROMID Study Group. *J. Clin. Oncol.* **27**, 4656–4663 (2009).
44. Imhof, A. et al. Response, survival, and long-term toxicity after therapy with the radiolabeled somatostatin analogue [90Y-DOTA]-TOC in metastasized neuroendocrine cancers. *J. Clin. Oncol.* **29**, 2416–2423 (2011).
45. Strosberg, J. et al. Phase 3 trial of (177)Lu-dotatate for midgut neuroendocrine tumors. *N. Engl. J. Med.* **376**, 125–135 (2017).
46. Pernas, S., Tolaney, S. M., Winer, E. P. & Goel, S. CDK4/6 inhibition in breast cancer: current practice and future directions. *Ther. Adv. Med. Oncol.* **10**, 1758835918786451 (2018).
47. Fujiwara, Y. et al. Phase 1 study of abemaciclib, an inhibitor of CDK 4 and 6, as a single agent for Japanese patients with advanced cancer. *Cancer Chemother. Pharmacol.* **78**, 281–288 (2016).
48. Ruscetti, M. et al. NK cell-mediated cytotoxicity contributes to tumor control by a cytostatic drug combination. *Science* **362**, 1416–1422 (2018).
49. Williams, B. O. et al. Cooperative tumorigenic effects of germline mutations in Rb and p53. *Nat. Genet.* **7**, 480–484 (1994).
50. Contractor, T. et al. Sexual dimorphism of liver metastasis by murine pancreatic neuroendocrine tumors is affected by expression of complement C5. *Oncotarget* **7**, 30585–30596 (2016).
51. Grant, S. G., Seidman, I., Hanahan, D. & Bautch, V. L. Early invasiveness characterizes metastatic carcinoid tumors in transgenic mice. *Cancer Res.* **51**, 4917–4923 (1991).
52. Rindi, G. et al. Development of neuroendocrine tumors in the gastrointestinal tract of transgenic mice. Heterogeneity of hormone expression. *Am. J. Pathol.* **136**, 1349–1363 (1990).